

We are IntechOpen, the world's leading publisher of Open Access books Built by scientists, for scientists

4,800

Open access books available

122,000

International authors and editors

135M

Downloads

Our authors are among the

154

Countries delivered to

TOP 1%

most cited scientists

12.2%

Contributors from top 500 universities



WEB OF SCIENCE™

Selection of our books indexed in the Book Citation Index
in Web of Science™ Core Collection (BKCI)

Interested in publishing with us?
Contact book.department@intechopen.com

Numbers displayed above are based on latest data collected.
For more information visit www.intechopen.com



Structure Based 3D-QSAR Studies on Cholinesterase Inhibitors

Zaheer ul Haq and Reaz Uddin

*Dr. Panjwani Center for Molecular Medicine and Drug Research, International Center for Chemical and Biological Sciences, University of Karachi
Pakistan*

1. Introduction

Alzheimer's disease (AD) is a slowly progressive neurodegenerative disorder of the elderly. It is characterized by widespread loss of central cholinergic neuronal function (Butters et al., 1995). The only symptomatic treatment proven to be effective to date is the use of cholinesterase inhibitors (ChEI) to augment surviving cholinergic activity (Giacobini, 2003, Terry & Buccafusco, 2003). Two types of ChE enzyme are found in the Central Nervous System (CNS), acetylcholinesterase (AChE; EC 3.1.1.7) and butyrylcholinesterase (BuChE; EC 3.1.1.8).

AChE and BuChE share 65% amino acid sequence homology despite being encoded by different genes on human chromosomes 7(7q22) and 3(3q26), respectively (Soreq & Zaku, 1993). Acetylcholinesterase is responsible for the hydrolysis of acetylcholine at the synaptic cleft and the neuromuscular junction in response to nerve action potential (Massoulie et al., 1993) while the BuChE preferentially acts on butyrylcholine, but also hydrolyzes acetylcholine (Cokugras, 2003). In addition, both AChE and BuChE seem to be involved in roles that are independent of their catalytic activities, such as cell differentiation and development (Behra et al., 2002, Meshorer et al., 2002). BuChE and AChE are able to catalyze the hydrolysis of acetylcholine (ACh) at a rate of >10,000 molecules per second (Bazelyansky et al., 1986).

Because BuChE is relatively abundant in plasma (about 3 mg/liter), and can degrade a large number of ester-containing compounds, it plays important pharmacological and toxicological roles (Lockridge & Masson, 2000). For instance, BuChE is a potential detoxifying enzyme to be used as a prophylactic scavenger against neurotoxic organophosphates such as the nerve gas soman (Lockridge & Masson, 2000, Massoulie et al., 1993, Xie et al., 2000).

Previously, the relative contribution of BuChE to the regulation of ACh levels was largely ignored presumably due to unclear physiological function of BuChE (Chatonnet & Lockridge, 1989, Mack & Robitzki, 2000, Massoulie, Pezzementi, 1993, Xie, Stribley, 2000). However, there is growing evidence that both enzymes regulate ACh levels and may also play a part in the development and progression of AD (Greig et al., 2001).

In the normal brain, AChE represents approximately 80% of ChE activity with BuChE comprising the remainder (Giacobini, 1964). In advanced AD, however, AChE activity may

be reduced to 55-67% of normal levels in specific brain regions, while BuChE activity increases (Giacobini, 1964, Greig, Utsuki, 2001, Mack & Robitzki, 2000). Cytochemical studies have revealed that in certain neuronal pathways of some species, BuChE replaces AChE (Graybiel & Ragsdale, 1982). The BuChE may also have a role in the aggregation of β -amyloid protein ($A\beta$) that occurs in the early stages of senile plaque formation in AD (Guillozet et al., 1997). Selective inhibition of BuChE versus AChE derives from an ability to utilize the additional space present in the gorge of BuChE.

From the resolved 3D structures of various cholinesterases, it is known that the active sites residues of these enzymes lay at the bottom of a 20 Å deep hydrophobic gorge (Bourne et al., 1995, Doorn et al., 2001, Harel et al., 1992, Nachon et al., 2005, Nicolet et al., 2003, Sussman et al., 1991, Tormos et al., 2005). Due to a large cavity of this gorge BuChEs accept in comparison to AChEs, broader variety of substrates and inhibitors (Radic et al., 1993, Saxena et al., 1999, Saxena et al., 1997). For instance they metabolize butyrylcholine, the choline ester with large acyl moiety whose hydrolysis by vertebrate AChEs is negligible.

Although a similar peripheral site has been described for human BuChE but site-directed mutagenesis and photo-affinity labeling studies showed that its location and the response upon ligand binding differ significantly from those of AChE (Graybiel & Ragsdale, 1982, Perry et al., 1978).

Structure-activity analysis is the foundation for understanding the structural features of both the inhibitors and the target receptors involved in particular biological process and thus helps to design more effective inhibitors (Cho et al., 1996). It appears relatively difficult to find a reliable predictive model based on the calculated energies obtained by docking (Donini & Kollman, 2000, Tame, 1999). To overcome this problem, highly predictive QSAR i.e., CoMFA (Cramer III et al., 1988) and CoMSIA (Klebe et al., 1994) modeling techniques have been developed by using the technique of structure-based alignments of the substrates. These models can be used to identify important protein-ligand interactions and are found to be consistent with the crystal structure of the protein-ligand complex (Prathipati et al., 2005). The availability of X-ray crystal coordinates of inhibitors bound with the receptor have contributed to formulate effective predictive 3D-QSAR models based on (1) identification of possible conformations of related inhibitors in the active site and (2) understanding of the interactions of the inhibitors with the receptor in three-dimension (Debnath, 1999). A 3D-QSAR experiment performs two functions: the derivation of a statistically significant and highly predictive model that is used to estimate and rank new compounds for planned synthesis and the provision of an easily interpretable graphical tool which can identify a particular physicochemical property for increased affinity and selectivity (Klebe, 1998). These physicochemical properties include steric bulk, partial charge, local hydrophobicity, or hydrogen bond donor and acceptor (Bohm et al., 1999).

The level-dependent contouring of usual CoMFA-field contributions highlights those regions in space where the aligned molecules would favourably or unfavourably interact with a possible environment. The CoMSIA field contributions identify those areas within the region occupied by the ligand that "favour" or "dislike" the presence of a group with a particular physicochemical property. This association of required properties with a possible ligand shape is a more direct indicator to check whether all features important for a particular activity are present in the structures under consideration (Klebe, Abraham, 1994).

The discovery of natural cholinesterase inhibitors has been a very challenging area of drug development due to the involvement of cholinesterases in Alzheimer's disease and other related dementias. We have previously reported a number of new natural inhibitors of

cholinesterases (AChE and BuChE) isolated from indigenous medicinal plants (Atta ur et al., 2000, Atta ur et al., 2004, Atta ur et al., 2004, Atta ur et al., 2002, Kalauni et al., 2001). The steady state inhibition kinetics, pharmacological profiles, SAR and molecular docking studies have been conducted on a similar series of compounds for AChE inhibition (Khalid et al., 2004, Khalid et al., 2004, Zaheer-Ul-Haq et al., 2003, Zaheer ul et al., 2003).

In the present study, two 3D-QSAR methods, CoMFA and CoMSIA, were applied and evaluated in order to accurately predict the inhibitory activity. For this reason a set of structurally similar cholinesterase inhibitors (both BuChE and AChE) were used to create a predictive model. The results from this study will be helpful for the design of new and more potent cholinesterase inhibitors.

Docking is one method in which the binding of an inhibitor to a receptor can be explored (Dominguez et al., 2003, Jain, 2003, Johnson et al., 2003, Sabnis et al., 2003, Todorov et al., 2003, Vicker et al., 2003, Wang et al., 2003, Wu et al., 2003, Zhou et al., 2003). In CoMFA or other 3D-QSAR studies, the molecule alignment and conformation determination are so important that they affect the success of a model. In the present case, a bound complex of steroidal alkaloid with cholinesterase was not available, and therefore, a computational method has to be implemented to determine possible conformations and alignment of a set of molecules so that 3D-QSAR can be carried out. Several strategies have been used in the past, to determine the conformation and alignment of molecules. Of them, docking is an attractive way to align molecules for CoMFA and/or CoMSIA. Several applications of docking alignment with CoMFA have been reported (Buolamwini & Assefa, 2002, Hu & Stebbins, 2005, Medina-Franco et al., 2004, Pan et al., 2006, Wei et al., 2005).

Recently, we used FlexX and FRED (FRED, 2007) to successfully dock a set of steroidal alkaloid inhibitors into the active site gorge of cholinesterase. A 3D-QSAR model was developed based on the docked conformation of the most active compound. In this paper we have performed CoMFA modeling utilizing the genetic algorithm (GA) in the selection of the ligand conformations. Previously this GA strategy has been utilized by Yuan and Zaheer ul Haq et al (Yuan et al., 2004, Yuan & Petukhov, 2006, Zaheer ul et al., 2008) and found that this is very efficient in terms of the reliability of the CoMFA models. GA is inspired by natural selection in evolution (Holland, 1975). GA approaches the optimum of a given function in the same way nature selects the individual fittest for the environment. The GA uses a blind search strategy, requiring no knowledge of the properties of the function to be optimized, thus enabling the algorithm to be applied to a variety of optimization problems from robot behavior to drug design (Fogel et al., 1966, Forrest, 1993, Goldberg, 1989).

2. Materials and methods

2.1 Biological data

The cholinesterase inhibitory activities, represented by IC_{50} (μM), were obtained from recently published data (Atta ur, Choudhary, 2000, Atta ur, Feroz, 2004, Atta ur et al., 2003, Atta ur et al., 1997, Atta ur, Zaheer ul, 2004, Atta ur, Zaheer ul, 2002, Kalauni, Choudhary, 2001, Khalid, Zaheer ul, 2004) (Table 1). The structures of inhibitors are presented in Table 2. The pIC_{50} ($-\log IC_{50}$) values were used to derive 3D-QSAR models. From a total of forty compounds, a training set was created with thirty five compounds (with the case of BuChE) and thirty three compounds (with the case of AChE) while other 5 compounds were used as the test set (Table 1). This test set was used to validate the predictive ability of the training set.

S. No.	Comp. No.	Compound Name	IC ₅₀ (μM) BuChE	IC ₅₀ (μM) AChE	pIC ₅₀ BuChE	pIC ₅₀ AChE
1	SAR01	Isosarcodine	1.89±0.06	10.31±0.13	5.72	2.99
2	SAR02	Iso-N-formylchoneformine	4.07±0.11	6.36±0.22	5.39	3.20
3	SAR03	Saracodinine	12.51±0.06	40.04±0.13	4.9	2.40
4	SAR04	Sarcorine	10.33±0.02	69.99±0.056	4.99	2.15
5	SAR05	N _a -Demethylsaracodine	16.55±0.20	204.2±4.951	4.78	1.69
6	SAR06	Saracocine	3.86±0.01	20±1.30	5.41	2.70
7	SAR07	Sarcodine	18.31±0.74	49.77±1.26	4.74	2.30
8	SAR08	Salignenamide-A	4.63±0.07	50.64±0.930	5.33	2.30
9	SAR09	Vaganine-A	2.32±0.06	8.59±0.155	5.63	3.07
10	SAR10	Saligcinnamide	4.84±0.12	19.99±0.123	5.32	2.70
11	SAR11	Salignenamide-C	38.36±0.74	61.3±2.02	4.42	2.21
12	SAR12	5,6-Dehydrosarconidine	1.89±0.06	20.29±1.82	5.72	2.69
13	SAR13	Salignamine	25.7±0.63	249±10.23	4.59	1.60
14	SAR14	Salignenamide-D	23.78±0.15	185.2±7.66	4.62	1.73
15	SAR15	Salignenamide-E	3.65±0.02	6.21±0.234	5.44	3.21
16	SAR16	Salignenamide-F	4.07±0.11	6.357±0.224	5.39	3.20
17	SAR17	2β-Hydroxyepipachysamine-D	28.96±0.01	78.2±2.325	4.54	2.11
18	SAR18 ^a	Salonine-B	4.50±0.07	-----	5.35	-----
19	SAR19	Salonine-A	32.70±1.20	33.4±3.21	4.49	2.48
20	SAR20	Salonine-C	32.20±0.50	7.8±0.5	4.49	3.11
21	SAR21	Salignarine-F	1.90±0.20	30.2±2.0	5.72	2.52
22	SAR22	16-Dehydrosarcorine	3.95±0.53	12.5±0.01	5.4	2.90
23	SAR23	Axillarine-C	17.99±0.22	227.92±8.677	4.74	1.64
24	SAR24	Axillarine-F	18.24±0.01	182.4±5.542	4.74	1.74
25	SAR25	Dictyophlebine	3.65±0.02	6.21±0.23	5.44	3.21
26	SAR26	Sarsalignenone	4.29±0.03	5.83±0.070	5.37	3.23
27	SAR27	Nepapakistamine	25.00±0.79	50.1±1.35	4.6	2.30
28	SAR28	Sarcoveganin-C	1.50±0.02	187.8±0.71	5.82	1.73
29	SAR29	Salignarine-C	1.25±0.01	19.7±0.05	5.9	2.71
30	SAR30	Sarsalignone	2.18±0.04	7.02±0.007	5.66	3.15
31	SAR31	N-Methylformamidesalonine-B	10.50±0.30	48.6±2.7	4.98	2.31
32	SAR32 ^a	5,14-dehydro-N _a -demethylsaracodine	25.00±0.60	-----	4.6	-----
33	SAR33	Axilliridine-A	2.49±0.06	5.21±0.105	5.6	3.28
34	SAR34	14-Dehydro-N _a -demtehylsaracodine	10.10±0.15	183.1±2.60	5	1.74
35	SAR35 ^t	Vaganine-D	10.00±0.120	46.89±1.94	5	2.33
36	SAR36 ^t	2-Hydroxysalignarin E	6.91±0.06	15.99±0.13	5.16	2.80
37	SAR37 ^t	Epipachysamine-D	2.82±0.02	28.93±0.54	5.55	2.54
38	SAR38 ^t	2-Hydroxysalignamine	20.95±3.20	82.5±2.22	4.68	2.08
39	SAR39 ^t	2,3-Dehydrosarsalignone	32.20±0.50	7.0±0.1	4.49	3.15
40	SAR40	Alkaloid C	22.13±0.14	42.2±0.26	2.65	2.37

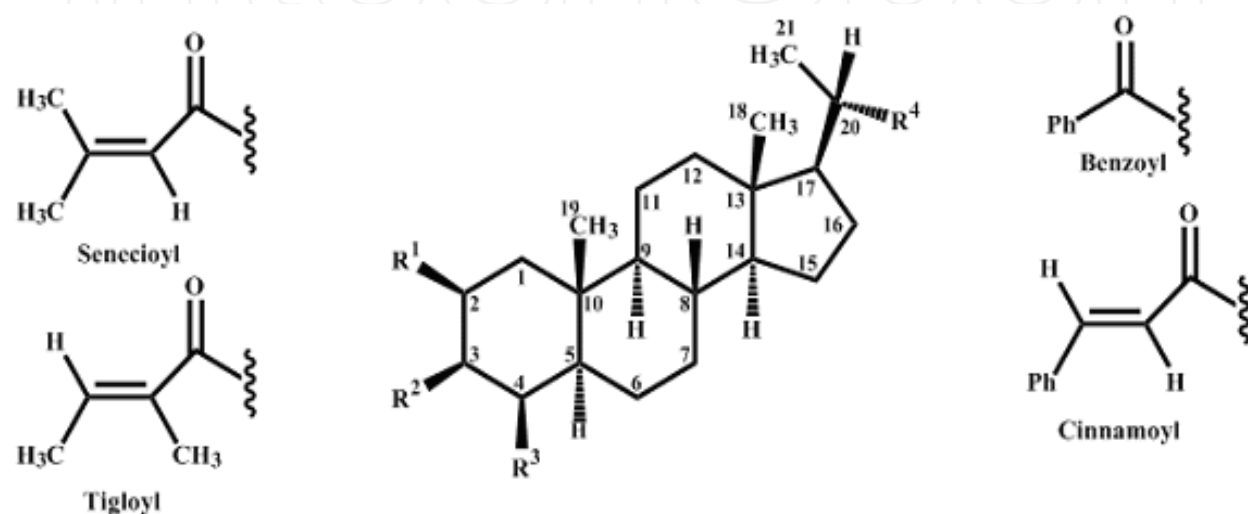
^t = test set

^a = not included in AChE modelling

Table 1. Inhibitory Activities of the Compounds

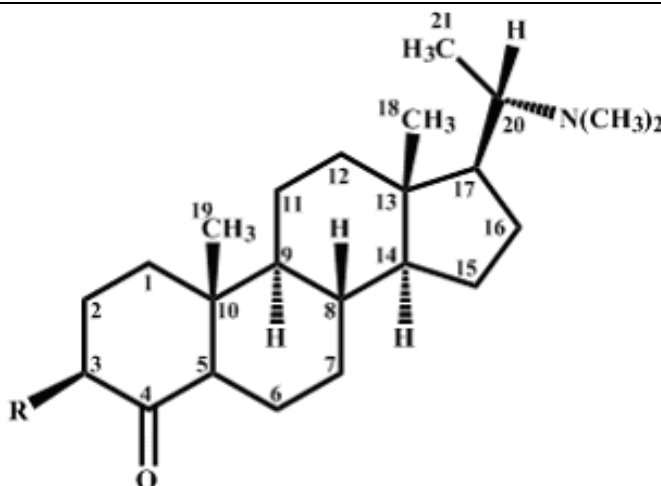
2.2 Modeling tools

All molecular modeling and comparative molecular field evaluations were performed using SYBYL 7.2 (Sybyl, 2007), running on AMD Athlon (tm) workstation. The aliphatic amine groups of all compounds were considered protonated. Geometry optimizations were performed using the Tripos forcefield (Clark et al., 1989) with a distance-dependent dielectric and the Powell conjugate gradient algorithm. Gasteiger Huckel charges were used. All water molecules, sulfate and chloride anions, glycerol, fucose, *N*-acetyl-*D*-glucosamine and 2-(*N*-morpholino)-ethanesulfonic acids were removed from the original protein data bank file.



Comp. No.	R ¹	R ²	R ³	R ⁴	Unsaturation
SAR01	H	NCH ₃ Ac	H	N(CH ₃) ₂	
SAR02	H	N(CH ₃) ₂	H	NHCHO	
SAR03	H	N(CH ₃) ₂	H	N(CH ₃) ₂	Δ ^{5,6}
SAR04	H	NHAc	H	N(CH ₃) ₂	
SAR05	H	NHCH ₃	H	NCH ₃ Ac	
SAR06	H	N(CH ₃) ₂	H	NCH ₃ Ac	Δ ^{5,6}
SAR07	H	N(CH ₃) ₂	H	NCH ₃ Ac	
SAR08	H	NHCOCH=C(CH ₃)CH(CH ₃) ₂	H	N(CH ₃) ₂	
SAR09	H	HN-Senecioyl	OAc	N(CH ₃) ₂	
SAR10	H	CH ₃ N-Cinnamoyl	H	N(CH ₃) ₂	
SAR11	OH	HN-Tigloyl	OAc	N(CH ₃) ₂	Δ ^{14,15}
SAR12	H	NHCH ₃	H	N(CH ₃) ₂	Δ ^{16,17}
SAR13	H	OCH ₃	H	NHCH ₃	Δ ^{5,6} & Δ ^{16,17}
SAR14	<i>α</i> -OH	HN-Tigloyl	H	N(CH ₃) ₂	Δ ^{4,5} & Δ ^{16,17}
SAR15	H	N(CH ₃)COCH=C(CH ₃)CH(CH ₃) ₂	H	N(CH ₃) ₂	Δ ^{16,17}
SAR16	H	N(CH ₃)COCH=C(CH ₃)CH(CH ₃) ₂	H	N(CH ₃) ₂	
SAR17	OH	HN-Benzoyl	H	N(CH ₃) ₂	
SAR18	H	OCH ₃	H	N(CH ₃) ₂	Δ ^{5,6} & Δ ^{16,17}
SAR19	OH	HN-Tigloyl	OH	N(CH ₃) ₂	Δ ^{14,15}
SAR20	H	HN-Tigloyl	H	N(CH ₃) ₂	Δ ^{4,5} & Δ ^{14,15}

SAR21	H	HN-Tigloyl	OH	N(CH ₃) ₂	Δ ^{5,6}
SAR22	H	NHCOCH ₃	H	N(CH ₃) ₂	Δ ^{16,17}
SAR23	OH	HN-Benzoyl	OAc	N(CH ₃) ₂	
SAR24	OH	HN-Tigloyl	OAc	N(CH ₃) ₂	
SAR25	H	NHCH ₃	H	N(CH ₃) ₂	
SAR27	OAc	HN-Tigloyl	OAc	NHCH ₃	Δ ^{16,17}
SAR29	OH	HN-Senecioyl	H	N(CH ₃) ₂	Δ ^{5,6}
SAR31	H	OCH ₃	H	NCH ₃ (CHO)	Δ ^{5,6} & Δ ^{16,17}
SAR32	H	NHCH ₃	H	NCH ₃ Ac	Δ ^{5,6} & Δ ^{14,15}
SAR34	H	NHCH ₃	H	NCH ₃ Ac	Δ ^{14,15}
SAR35	H	HN-Senecioyl	OAc	N(CH ₃) ₂	Δ ^{16,17}
SAR36	OH	HN-Tigloyl	H	N(CH ₃) ₂	Δ ^{4,5}
SAR37	H	HN-Benzoyl	H	N(CH ₃) ₂	
SAR38	OH	OCH ₃	H	N(CH ₃) ₂	Δ ^{5,6} & Δ ^{16,17}
SAR40					



Comp. No.	R	Unsaturation
SAR26	HN-Tigloyl	Δ ^{5,6} & Δ ^{14,15}
SAR28	HN-Tigloyl	Δ ^{2,3} & Δ ^{16,17}
SAR30	HN-Tigloyl	Δ ^{5,6}
SAR33	HN-Benzoyl	Δ ^{2,3}
SAR39	HN-Tigloyl	Δ ^{2,3} & Δ ^{5,6}

Table 2. Chemical Structures of the Compounds

2.3 Docking

FlexX, incremental construction algorithm (Rarey et al., 1996), was used to choose the appropriate binding conformations of the steroidal alkaloids inhibitors into the BuChE binding pocket. The crystal structure of human BuChE (pdb code: 1P0I) was used. One of the most active compound, SAR29 (see Table 2), was docked into the binding pocket and the best conformation was used as a template to align rest of the compounds. The FlexX scoring function was used to select the best conformation. Prior to dock the inhibitors with protein crystal structure, a re-docking of co-crystallized ligand with 1P0I was performed to validate

the docking protocol. The top most docked solution was found in good agreement with the crystal structure of the co-crystallized ligand. The RMSD between the docking solution and the crystal structure was 1.53 Å.

Molecular docking with AChE was carried out using FRED docking program. FRED (Fast Rigid Exhaustive Docking) is a protein-ligand docking program, which takes a multiconformer library/database and receptor file as input and output molecules of the input database most likely to bind to the receptor (FRED, 2007, McGann et al., 2003).

First stage in FRED docking is a shape fitting process, which takes a set of ligand conformers as input and tests them against a "bump map" (a Boolean grid with true values where ligand atoms can potentially be placed). Orientations that clash with the protein or are distant from the active site are rejected. The crude docking solutions are further tested against a pharmacophore feature if specified and any poses that do not fit in the pharmacophore criteria are rejected. Poses surviving the shape fitting routine can then be passed through up to three scoring function filters in the screening process. Available scoring functions in FRED are ChemScore, PLP, ScreenScore, and Gaussian shape fitting (McGann, Almond, 2003).

2.4 Conformational sampling and alignment

The selected poses for SAR29 (one of the most active compound against BuChE) and SAR33 (one of the most active compound against AChE) were used as templates in structure alignment for all molecules in the respective series. For BuChE, this step was performed by using an incremental construction algorithm and a scoring function based on intermolecular interactions and overlapping density functions implemented in the Flexible Superposition (FlexS) technique (Lemmen et al., 1998). The minimum volume overlap was set at 0.6 and the number of alignments per ligand was used initially as 30 (default) but was changed for the cases where optimum alignment was not obtained. The Gasteiger Huckel charges were calculated during conformational alignment with FlexS. A top-ranked conformer for each compound was initially utilized for CoMFA modeling and then the ten best conformations were used in order to explore all possible conformational space for each compound. The ten best poses were selected based on the following:

1. FlexS ranks and
2. If the pose is correctly oriented on the template.

The Figure 1a represents the alignment of the molecules using SAR29 as a template for BuChE modeling.

In the case of AChE, the superimposition was performed using the ROCS from openeyes (OE ROCS, 2008). The ROCS is a Rapid Overlay on Crystal Structures (ROCS). ROCS method has a number of applications in virtual screening, lead hopping and in 3D-QSAR. ROCS can be utilized as an alignment method in order to produce the conformations which subsequently can be utilized in conformations sensitive 3D-QSAR i.e. CoMFA. The ROCS was used with its default settings except the maximum numbers of conformations and numbers of best hits to be saved were 30 and 1000, respectively. ROCS overlays the multiconformer compound's database in shape and chemistry with respect to the reference ligand. The overlays can be performed very quickly based on a description of the molecules as atom-centered Gaussian functions. ROCS maximizes the shared volume between a query molecule and a single conformation of a database molecule. Figure 1b represents the alignment of the molecules using SAR33 as a template for AChE modeling.

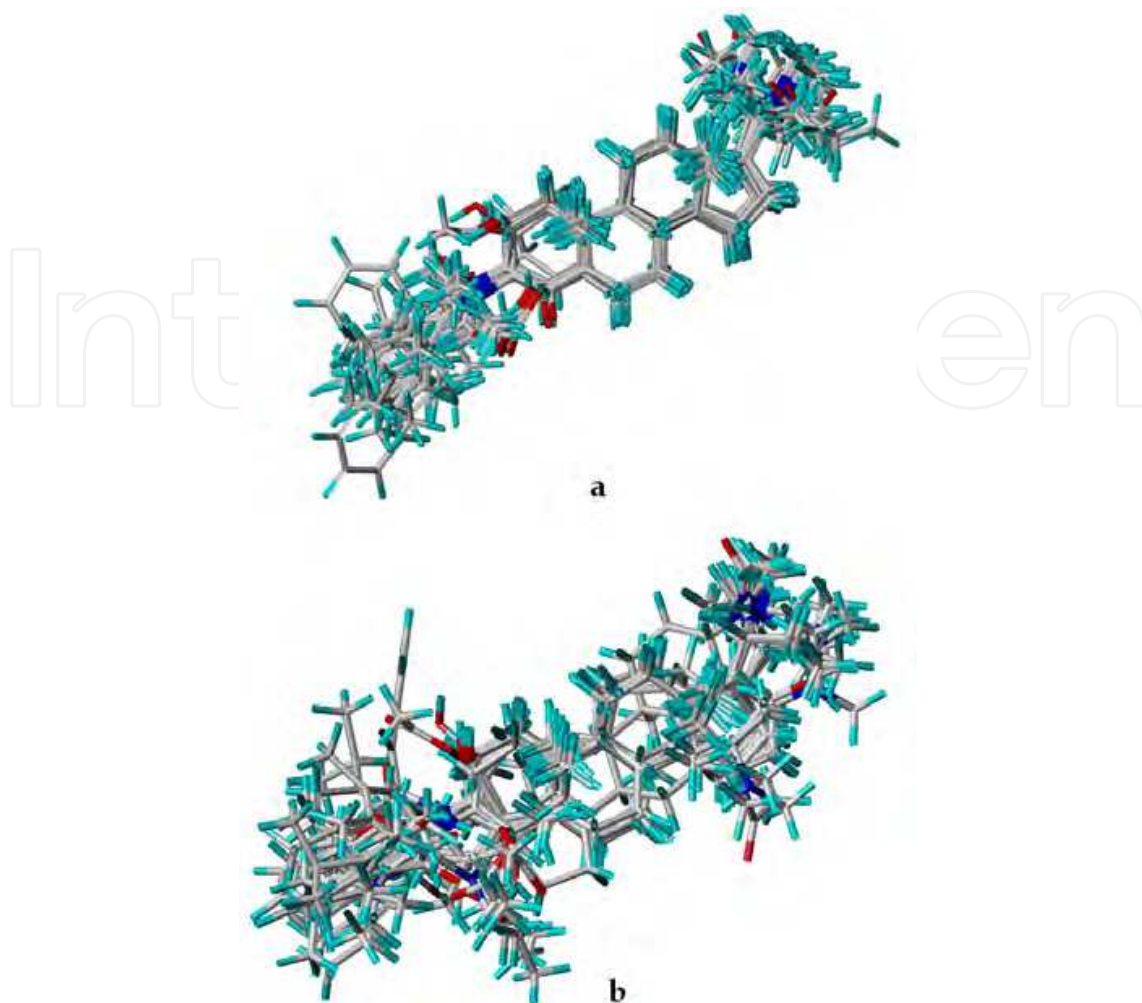


Fig. 1. Superposition of all studied inhibitors: a) BuChE using SAR29 as template b) AChE using SAR 33 as template

2.5 CoMFA modeling based on genetic algorithm

The overall strategy for CoMFA GA modeling is shown as a scheme in Figure 2. A brief description of the procedure is outlined here. To explore the multiple conformations of the ligands, a genetic algorithm analysis was applied in the selection of ligand's conformations for CoMFA. The genetic algorithm consisted of the following steps:

Initialization: This step generates an initial population P_i of CoMFA models using one randomly selected conformation among pre-filtered conformations of each ligand. The population size was set to 100.

Iterations:

Crossover: Exchange the conformations of corresponding ligands for any two models in the population P_i . The crossover ratio was set to 50:50.

Mutation: For randomly selected ligands, replace the conformations obtained in step 1 with randomly selected conformations in the database. Store the results as a temporary population P_{tmp} . The mutation rate was set to 0.05.

Selection: Generate new CoMFA models for P_{tmp} . Compare their q^2 values with those generated for population P_i and keep the best models in population P_{i+1} .

Until: The 100 generations limit is reached or the best model remains unchanged for 10 consecutive generations.

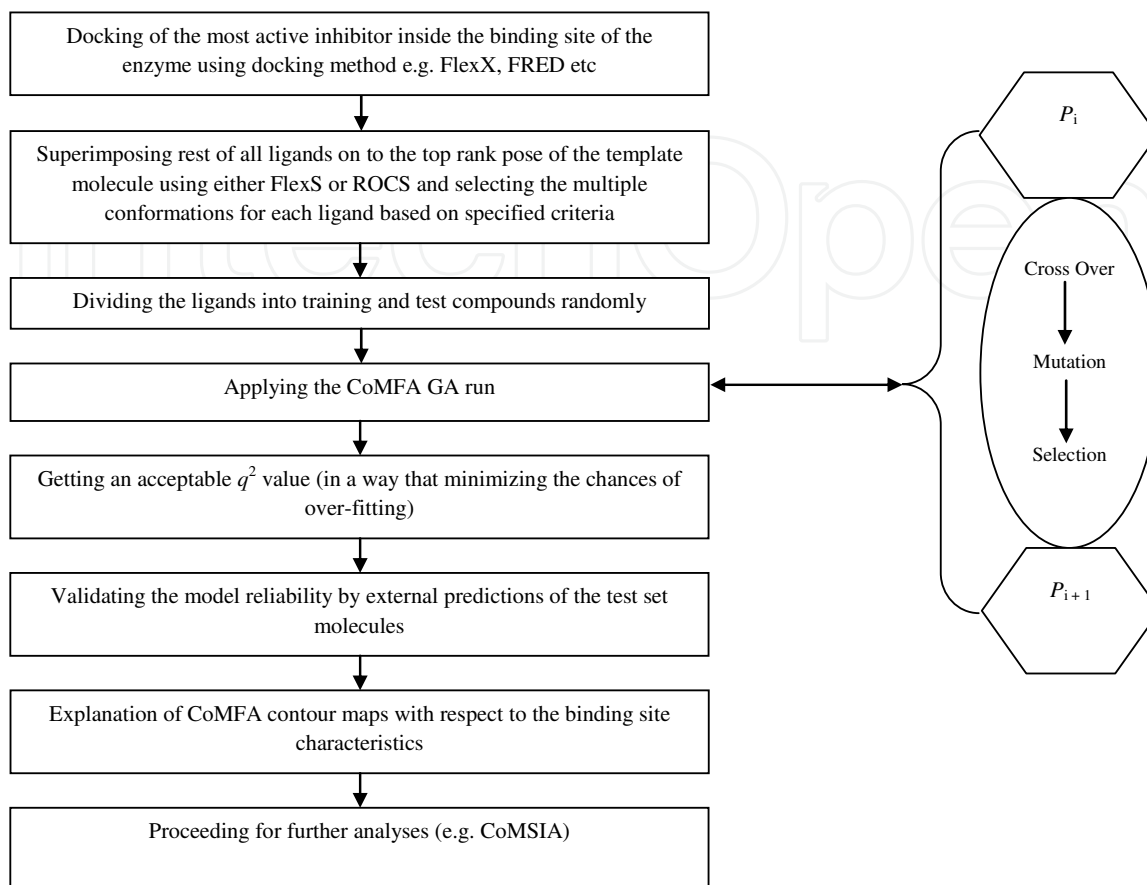


Fig. 2. Scheme for overall procedure applied during GA based 3D-QSAR modeling

2.6 CoMFA fields

Training sets of, thirty five compounds (with the case of BuChE) and thirty three compounds (with the case of AChE; see Table 1), were selected from the existing database, representing the diversity of structures and activities. After alignment, the molecules were inserted as rows of a QSAR table along with their respective IC_{50} values (as pIC_{50}). CoMFA steric and electrostatic fields were calculated as described below and entered as columns in the QSAR table. Standard steric and electrostatic CoMFA field energies of each inhibitor were calculated using an sp^3 probe atom with a +1 charge at all intersections in regularly spaced (2.0 Å) grids surrounding each molecule. Lennard Jones 6-12 potential and coulombic potential functions, within the Tripos forcefield (Clark, Cramer, 1989) and a distance dependent (1/r) dielectric constant were used in the calculation. The grid box dimensions were determined by the “create automatically” features in the CoMFA module within the “SYBYL” program. The same grid box was used in all calculations. An energy cutoff of 30 kcal/mol for both steric and electrostatic contributions was set as threshold and the electrostatic terms were dropped within regions of steric maximum i.e., 30 kcal/mol. Five additional inhibitors (Table 1) were selected as a predictive set to test the robustness of the resulting model. They were aligned with template structures using the same alignment protocol as described earlier and finally their activities were predicted.

2.7 CoMSIA fields

Another 3D-QSAR procedure, CoMSIA can avoid some inherent deficiencies arising from the functional forms of Lennard-Jones and Coulomb potentials used in CoMFA. In CoMSIA, a distance dependent Gaussian-type functional form has been introduced. This can avoid singularities at the atomic positions and the dramatic changes of potential energy due to grids in the proximity of the surface. Meanwhile, no arbitrary definition of cut-off limits is required in CoMSIA and the contour maps of the relative spatial contributions of the different fields can be substantially improved. This is essential for the interpretation in terms of separate property fields. The procedures of getting a 3D-QSAR model from a CoMSIA can be summarized into following three steps.

First, all molecules are structure-based or field-based aligned.

Then, an evenly-spaced rectangular grid is generated to enclose the molecular aggregate. A probe atom is placed at every lattice point to measure the electrostatic, steric, hydrophobic, and H-bond donor or acceptor fields.

Finally, the results from the field samplings are combined with the biological activities from the tested compounds are put into a table and partial least squares (PLS) fitting is applied to obtain the final CoMSIA model.

To choose the appropriate components and to check the statistical significance of the models, leave-one-out cross-validations were used by PLS. Then, the final 3D-QSAR model was derived from no cross-validation calculations. The CoMSIA results are finally interpreted graphically by field contribution maps using the field type "stdev*coeff".

Similar to the usual CoMFA approach, a data table has been constructed from similarity indices (Klebe, 1998) calculated via a common probe atom that is placed at the intersections of a regularly spaced lattice. A grid spacing of 2 Å has been used throughout this study. Similarity indices $A_{F,K}$ between the compounds of interest and a probe atom, systematically placed at the intersections of the lattice, have been calculated according to equation 1 (e.g., at grid point q for molecule j of the data set).

$$A_{FK}^q(j) = -\sum_i \omega_{probe,k} \omega_{ik} (e^{-ar})^2 \quad (1)$$

Where i = summation index over all atoms of the molecule j under investigation; ω_{ik} = actual value of the physicochemical property k of atom i ; $\omega_{probe,k}$ = probe atom with charge +1, a = attenuation factor; and r_{iq} = mutual distance between probe atom at grid point q and atom i of the test molecule. Large values of a will result in a strong attenuation of the distance-dependent consideration of molecular similarity. Accordingly, there is little averaging of local feature matches of the molecules being compared. With small values of a , also remote parts of each molecule will be experienced by the probe and the global molecular features become more important. In the present study the a has been set at 0.3. With this selection, at a given lattice point the property value of an atom of the molecule under investigation (e.g., the partial atomic charge) is experienced in 1 Å distance by 74.1%, in 2 Å by 30.1% and in 3 Å by 6.7% of its total value. This permits a reasonable "local smearing" of the molecular similarity indices and should help to avoid extreme dependencies on small changes of the mutual alignments (Bohm, St rzebecher, 1999). In the present study five physicochemical properties k (steric, electrostatic, hydrophobic and hydrogen bond donor and acceptor) were evaluated, using a common probe atom with 1 Å radius and charge, hydrophobicity and hydrogen-bond property of +1. Steric property fields were expressed by the third power of the atomic radii. Local hydrophobicities were associated using atom-based parameters developed by Viswanadhan et al (Viswanadhan et al., 1989).

2.8 Statistical analysis/PLS

Correlations were derived using the method of Partial Least Squares (PLS) (Geladi & Kowalski, 1986) and cross validated to reduce the probability of obtaining chance correlations. As used in this report, the cross-validated q^2 refers to the squared correlation coefficient of the equation derived from the cross-validation of the training set to determine the optimum number of principal components. The conventional r^2 is the fitted correlation of the training set using the optimum number of principal components with no cross validation. The predictive r -squared was calculated by the equation 2.

$$\text{predictive } r\text{-squared} = \frac{\text{SSD} - \text{PRESS}}{\text{SSD}} \quad (2)$$

Where SSD is sum of squared deviations and PRESS is predictive residual sum of squares.

3. Results and discussion

3.1 Docking

The best docking poses for SAR29 and SAR33 inside the binding pockets of BuChE and AChE are shown in Figure 3a and 3b, respectively. The poses indicated that the ligands were

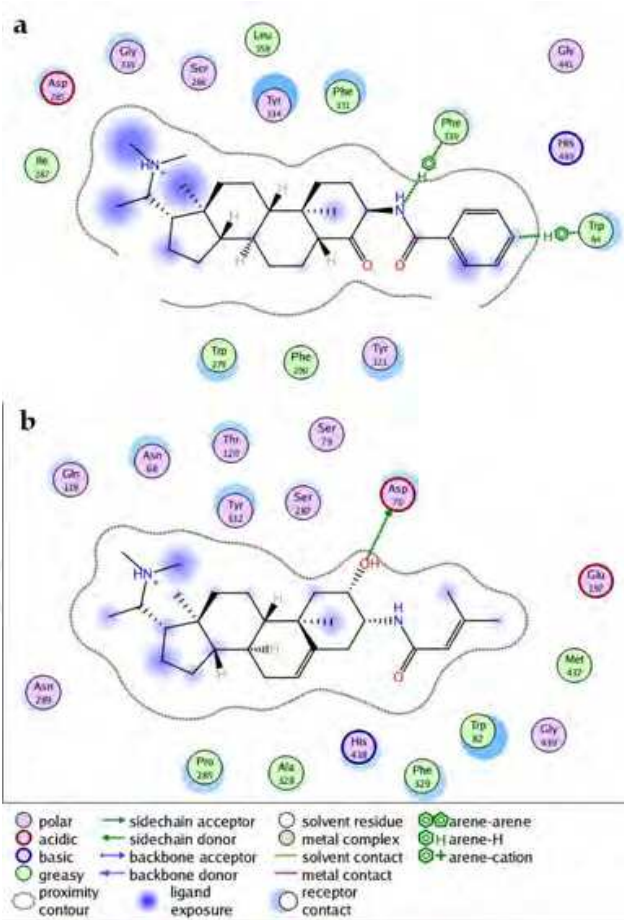


Fig. 3. Docked poses of most active compound **a)** SAR29 for BuChE and **b)** SAR33 for AChE within the surrounding binding site residues. The figures are rendered by MOE Ligand interaction

accommodated well inside the binding sites. The compound enters the cavity preferably by ring A. This might contribute highly to the stabilization of the complex since the steroid backbone of the ligand is highly hydrophobic due to its aliphatic character and therefore, not well hydrated. The main hydrophobic interactions between the hydrocarbon skeleton of the inhibitors and the cholinesterases binding sites were observed with the most common residues i.e. Thr, Tyr, Trp, Ala, and Phe.

3.2 3D-QSAR of inhibitors

3.2.1 Model selection

The CoMFA based on GA, resulted in several models and among them, the final model selection is an important issue. With the case of BuChE, four different models have been selected based on q^2 values. Among them, models 72 and 80 were obtained with the cutoff $q^2 \geq 0.65$; and the other two models 9 and 21, with the cutoff $q^2 \geq 0.90$ (Table 3).

Parameters	Model9	Model21	Model72	Model80
q^2 ^a	0.902	0.911	0.730	0.701
r^2 ^b	0.998	0.998	0.994	0.979
SEE ^c	0.022	0.020	0.040	0.072
F-value ^d	2326.92	2957.134	738.562	264.356
No. of Components ^e	6	6	6	5
Fraction ^f				
Steric	0.499	0.484	0.500	0.531
Electrostatic	0.501	0.516	0.500	0.469
Predictive r -Squared ^g	0.441	0.523	0.311	0.682
PRESS ^h	0.384	0.328	0.475	0.218

^a Cross-validated correlation coefficient.

^b Noncross-validated correlation coefficient.

^c Standard error of estimate.

^d F-test value.

^e Optimum number of components obtained from cross-validated PLS analysis and same used in final non-cross-validated analysis.

^f Field contributions.

^g Correlation coefficient for test set predictions.

^h Predicted residual sum of squares.

Table 3. Summary of Statistics and Field Contributions for the Top Four CoMFA Models with the case of BuChE

The external predictivity of the CoMFA model is extremely important in terms of the applicability of the CoMFA model. Therefore, it was decided to use the predictive- r^2 as a criterion for final selection of the one best model. As reflected by the Table 3, model 80 has the highest predictive- r^2 value and hence the lowest PRESS value for the test set predictions. Therefore, model 80 was selected as the best CoMFA model. In addition, to study the effect of charges on 3D-QSAR studies, different methods were employed to calculate the charges on ligands included in this study. Quantitative comparisons of the charges calculated by different methods are reported in Table 4. Different charges resulting from different

calculation methods may influence the results of CoMFA as well as CoMSIA, but there is no significant effects of charges observed during our study for this particular steroidal class of compounds.

With the case of AChE, another way of model selection was done. In each case of GA run the predictive- r^2 was also calculated and compared it with each generation's top model. The default settings of 100 individuals and 100 generations were used but the GA resulted in early termination with 28th generation due to achieving the cutoff value of fitness function (i.e. $q^2 = 0.80$). The graphical representation is presented in Figure 4. The generation number six (highlighted in circle in Figure 4) was the first in identifying the acceptable q^2 as well as the predictive r^2 . Hence, the model number six was utilized for further analysis with the case of AChE.

S.No.	Charges Method	CoMFA			CoMSIA		
		q^2	r^2	Components	q^2	r^2	Components
1	Gasteiger Marsilli	0.696	0.989	6	0.636	0.980	5
2	Gasteiger Huckel	0.701	0.979	5	0.627	0.982	5
3	Huckel	0.673	0.988	5	0.637	0.981	5
4	MMFF94	0.716	0.993	6	0.669	0.986	4
5	Pullman	0.697	0.989	6	0.630	0.981	5
6	Delre	0.680	0.987	5	0.634	0.980	6

Table 4. Influence of Different Charges on BuChE Predictive Model

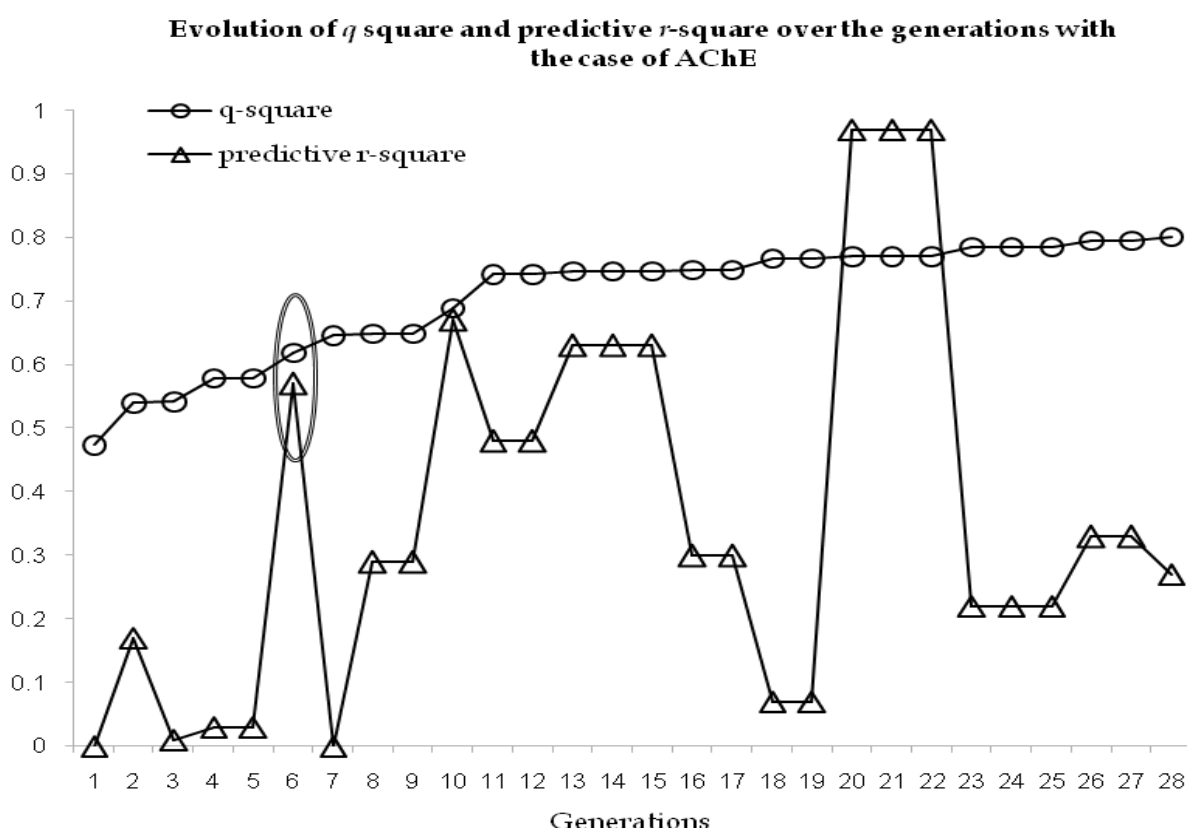


Fig. 4. Comparison between q^2 and predictive r^2 over the generations with AChE modeling

3.2.2 Predictive power of the 3D-QSAR model

The final results of CoMFA and CoMSIA analysis in both cases (i.e. BuChE and AChE) with 2.0 Å grid spacing are shown in Table 5 and Table 6, respectively. PLS analysis yielded consistent results. The optimal components that produce the best cross-validation linear regression coefficient were used to produce the non-cross-validated model. The inhibitory activities (pIC_{50}) and the calculated activities using CoMFA and CoMSIA models for training set and test set are listed in Table 7. Graphic representation of observed vs calculated inhibitory activity is shown in the Figure 5. Best selected 3D-QSAR models showed good prediction for five tested compounds, which reflects that the derived models were satisfactory enough in respect to statistical significance and actual predictive ability.

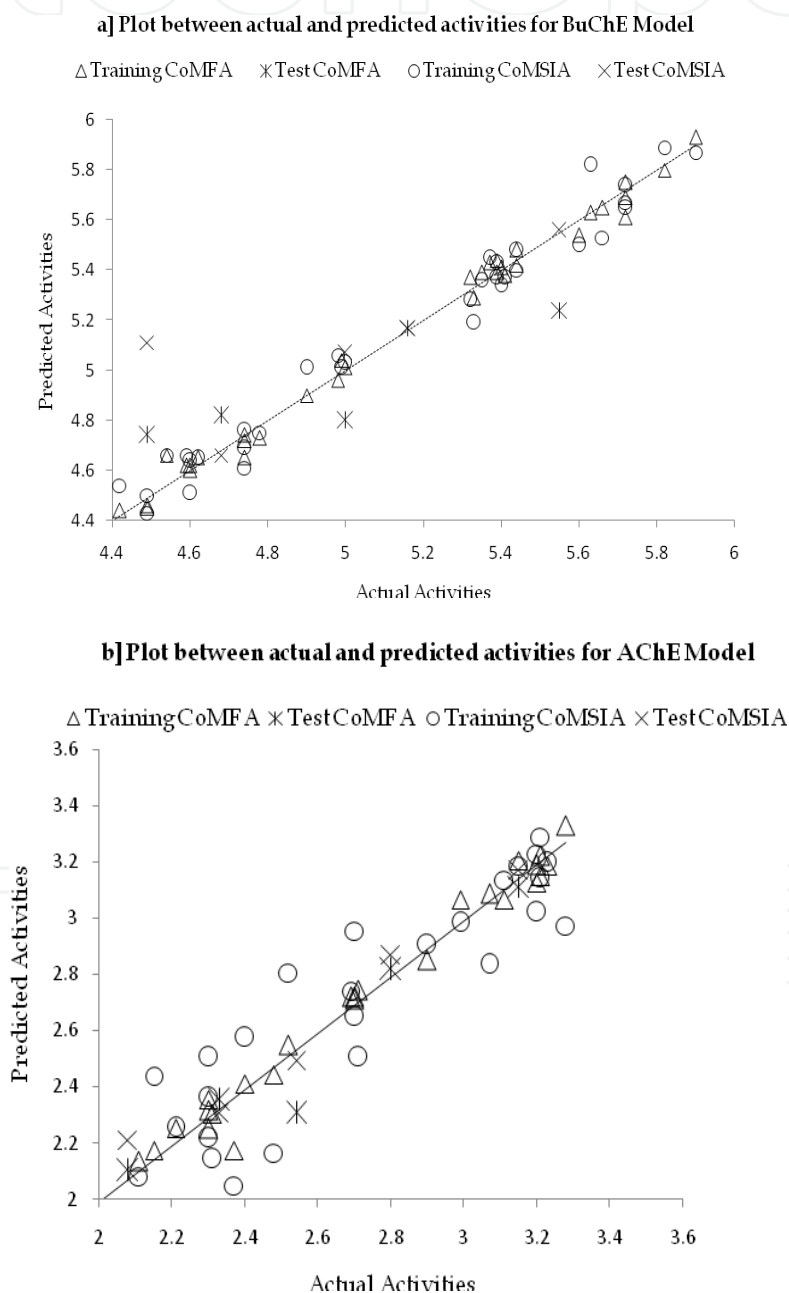


Fig. 5. Plots of the predicted versus experimental activity data of 3D-QSAR from both CoMFA and CoMSIA for training and test compounds a) BuChE and b) AChE

Parameters	CoMFA	CoMSIA				
	S, E ^(h)	S, E, H, D, A ^(h)	S, E ^(h)	S, E, H ^(h)	S, E, H, A ^(h)	S, E, H, D ^(h)
q^2 ^a	0.701	0.627	0.382	0.444	0.386	0.615
SEP ^b	0.273	0.305	0.393	0.373	0.392	0.310
No. of Components ^c	5	5	5	5	5	5
r^{2d}	0.979	0.982	0.880	0.927	0.924	0.967
SEE ^e	0.072	0.085	0.174	0.135	0.138	0.090
Field Contributions	0.531, 0.469	0.064, 0.173, 0.135, 0.373, 0.255	0.330, 0.670	0.211, 0.393, 0.396	0.122, 0.237, 0.251, 0.390	0.102, 0.246, 0.197, 0.456
F-value ^f	264.356	185.867	40.877	70.649	68.035	166.192
Predictive r -squared ^g	0.682	0.453	0.228	0.529	0.048	0.774

^a Cross-validated correlation coefficient.

^b Standard error of predictions.

^c Optimum number of components obtained from cross-validated PLS analysis and same used in final non-cross-validated analysis.

^d Noncross-validated correlation coefficient.

^e Standard error of estimate.

^f F-test value.

^g Correlation coefficient for test set predictions.

^h CoMFA and CoMSIA with different field contributions such as steric (S), electrostatic (E), hydrophobic (H), donor (D), and acceptor (A) fields.

Table 5. Results of CoMFA and CoMSIA Analyses for Compounds Used in Training Set (BuChE modeling)

Parameters	CoMFA	CoMSIA				
	S, E ^(h)	S, E, H, D, A ^(h)	S, E ^(h)	S, E, H ^(h)	S, E, H, A ^(h)	S, E, H, D ^(h)
q^2 ^a	0.632	0.630	0.661	0.641	0.650	0.636
SEP ^b	0.374	0.355	0.359	0.370	0.358	0.359
No. of Components ^c	6	3	6	6	5	4
r^2 ^d	0.989	0.909	0.979	0.984	0.966	0.947
SEE ^e	0.066	0.176	0.090	0.078	0.111	0.136
Field Contributions	0.524, 0.476	0.066, 0.237, 0.114, 0.307, 0.276	0.201, 0.799	0.139, 0.568, 0.293	0.095, 0.349, 0.160, 0.396	0.087, 0.341, 0.172, 0.401
F-value ^f	377.882	96.415	220.40	269.126	154.86	125.930
Predictive r -squared ^g	0.964	0.985	0.877	0.917	0.954	0.888

^a Cross-validated correlation coefficient.

^b Standard error of predictions.

^c Optimum number of components obtained from cross-validated PLS analysis and same used in final non-cross-validated analysis.

^d Noncross-validated correlation coefficient.

^e Standard error of estimate.

^f F-test value.

^g Correlation coefficient for test set predictions.

^(h) CoMFA and CoMSIA with different field contributions such as steric (S), electrostatic (E), hydrophobic (H), donor (D), and acceptor (A) fields.

Table 6. Results of CoMFA and CoMSIA Analyses for Compounds Used in Training Set (AChE modeling)

S.No.	Compound	Actual pIC_{50} <i>BuChE</i>	CoMFA Predicted pIC_{50} <i>BuChE</i>	CoMSIA Predicted pIC_{50} <i>BuChE</i>	Actual pIC_{50} <i>AChE</i>	CoMFA Predicted pIC_{50} <i>AChE</i>	CoMSIA Predicted pIC_{50} <i>AChE</i>
Training set							
1	SAR01	5.72	5.61	5.65	2.99	3.07	2.98
2	SAR02	5.39	5.44	5.43	3.2	3.13	3.23
3	SAR03	4.90	4.90	5.01	2.4	2.41	2.58
4	SAR04	4.99	5.04	5.01	2.15	2.18	2.44
5	SAR05	4.78	4.73	4.75	1.69	1.69	1.75
6	SAR06	5.41	5.38	5.37	2.70	2.71	2.65
7	SAR07	4.74	4.72	4.76	2.30	2.32	2.36
8	SAR08	5.33	5.29	5.19	2.30	2.25	2.51
9	SAR09	5.63	5.63	5.82	3.07	3.09	2.84
10	SAR10	5.32	5.37	5.28	2.70	2.72	2.95
11	SAR11	4.42	4.44	4.54	2.21	2.25	2.26
12	SAR12	5.72	5.75	5.67	2.69	2.72	2.74
13	SAR13	4.59	4.62	4.66	1.60	1.76	1.72
14	SAR14	4.62	4.65	4.65	1.73	1.68	1.71
15	SAR15	5.44	5.42	5.48	3.21	3.15	3.14
16	SAR16	5.39	5.39	5.37	3.20	3.19	3.02
17	SAR17	4.54	4.66	4.66	2.11	2.13	2.08
18	SAR18 ^a	5.35	5.39	5.36	-----	-----	-----
19	SAR19	4.49	4.45	4.43	2.48	2.44	2.17
20	SAR20	4.49	4.46	4.50	3.11	3.07	3.14
21	SAR21	5.72	5.69	5.74	2.52	2.55	2.81
22	SAR22	5.40	5.41	5.34	2.90	2.85	2.91
23	SAR23	4.74	4.74	4.69	1.64	1.60	1.79
24	SAR24	4.74	4.65	4.61	1.74	1.71	1.89
25	SAR25	5.44	5.48	5.40	3.21	3.22	3.29
26	SAR26	5.37	5.43	5.45	3.23	3.19	3.20
27	SAR27	4.60	4.62	4.64	2.30	2.36	2.22
28	SAR28	5.82	5.80	5.89	1.73	1.74	1.89
29	SAR29	5.90	5.93	5.87	2.71	2.74	2.51
30	SAR30	5.66	5.65	5.53	3.15	3.20	3.19
31	SAR31	4.98	4.96	5.06	2.31	2.30	2.14
32	SAR32 ^a	4.60	4.60	4.51	-----	-----	-----
33	SAR33	5.60	5.54	5.50	3.28	3.33	2.97
34	SAR34	5.00	5.01	5.03	1.74	1.77	1.58
35	SAR40	2.65	2.613	2.620	2.37	2.18	2.05
Test set							
36	SAR35	5.00	4.80	5.07	2.33	2.35	2.31
37	SAR36	5.16	5.17	5.17	2.80	2.82	2.87
38	SAR37	5.55	5.24	5.56	2.54	2.31	2.49
39	SAR38	4.68	4.82	4.66	2.08	2.10	2.21
40	SAR39	4.49	4.74	5.11	3.15	3.11	3.17

^a = not included in AChE modeling

Table 7. Comparisons of Experimental and Calculated Biological Activities of the Compounds by Using CoMFA and CoMSIA Analyses

3.2.3 Graphical interpretation of the results (CoMFA)

3.2.3.1 BuChE

CoMFA steric and electrostatic fields from the final non-cross-validated analysis were plotted as three-dimensional colored contour maps in Figure 6a. The field energies at each lattice point were calculated as the scalar results of the coefficient and the standard deviation associated with a particular column of the data table ($\text{stdev} \times \text{coeff}$), plotted as the percentage of contribution to the CoMFA equation. These maps show regions where differences in molecular fields are associated with differences in biological activity.

The steric interactions are represented by green and yellow colors while electrostatic interactions are represented by red and blue colors (Figure 6a). In the green regions of steric contour plot, bulky substituent enhances biological activity while bulky substituent in the yellow region is likely to decrease activity. The green steric contour near the substituent at C20 of the D ring indicates that any bulky substituent is preferred at this position. This may provide more possibilities to establish hydrophobic interactions with peripheral site of the target protein. This observation is consistent with the experimental findings as compound SAR13 is less active than SAR38 because SAR13 is having less bulky substituent at C20 than SAR38.

In electrostatic contour map blue-colored contours represent regions where electropositive groups increase activity whereas red colored regions represent areas where electronegative groups enhance activity. The electrostatic contour plot on the set of compounds showed that there is a red-colored region situated close to the substituent at C3 that is to say, the negative charges at this region are in a high demand for ligand binding and a charge withdrawing group linked to this position will enhance the biological activity. This observation also correlates with the experimental determinations, for example, the compound SAR37 is more active than compound SAR17. The only difference in both of them is the presence of a hydroxyl group at C-2 in compound SAR17 which makes SAR17 less active than SAR37 since C2 position is covered by the blue contour map. On the other hand a negative group at C-4 position makes compound SAR26, SAR28, SAR30, and SAR33 the most active compounds among the listed compounds. The presence of a double bond between C-5 and C-6 makes compound SAR06 more active than compound SAR07, which has otherwise identical structure.

3.2.3.2 AChE

In Figure 7a it is possible to observe two well-defined zones (close to the substituent at position C-4 and side chain at C-3 position) in which the presence of negative density favors an increase of AChE inhibitory activity. Furthermore, the presence of a double bond in ring B, between C-5 and C-6, also increases the activity. Small zones near C-2 have an opposite effect, that is, a negative density decreases the activity: for example, the only difference between compounds SAR17 and SAR37 is the presence of a hydroxyl group at C-2, which makes compound SAR17 less active than SAR37, on the other hand a negative group at C-4 position makes compounds SAR33, SAR30 and SAR26 the most active compounds in our study. Similarly, the presence of a double bond between C-5 and C-6 makes compound SAR06 more active than compound SAR07 which has an otherwise identical structure. Figure 7a displays two big zones near position C-4 and near the side chain at C-3, where the presence of bulky substituents decreases the activity. The region between C14 and C15 is also not favorable for bulky groups, which assigns a further role to the presence of the double bond in ring D as it means the lack of a further substitution. This difference can be easily seen by comparing compounds SAR30 and SAR26.

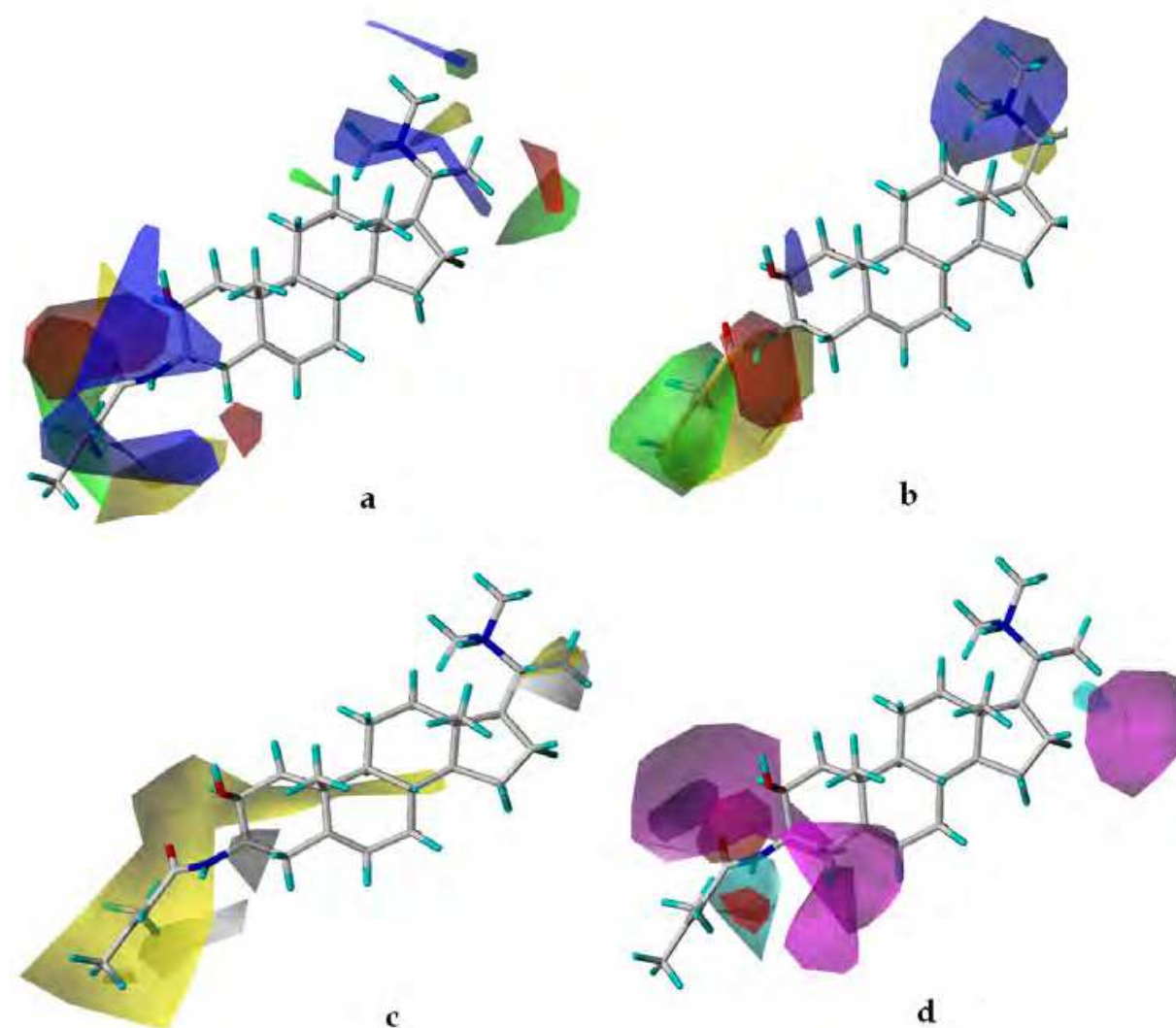


Fig. 6. **a**) The CoMFA (stdev*coeff) steric and electrostatic contour plots for BuChE modeling. The favorable steric areas in green; disfavored steric areas in yellow. The positive potential favored area in blue; positive potential disfavored areas in red. The most active compound in the series (SAR29) is shown as the reference compound. **b**) The CoMSIA (stdev*coeff) steric and electrostatic contour plots. Color scheme same as in figure 6a. The most active compound in the series (SAR29) is shown as the reference compound. **c**) The CoMSIA (stdev*coeff) hydrophobic contour plots. The favorable hydrophobic areas indicated by yellow color, whereas the disfavored hydrophobic areas are shown by white color. The most active compound (SAR29) is shown as the reference compound. **d**) The contour plots of the CoMSIA (stdev*coeff) H-bond donor and acceptor fields. The favorable H-bond donor in cyan; unfavorable H-bond donor in purple. The favorable H-bond acceptor in magenta; unfavorable H-bond acceptor in red. The most active compound (SAR29) is shown as the reference compound

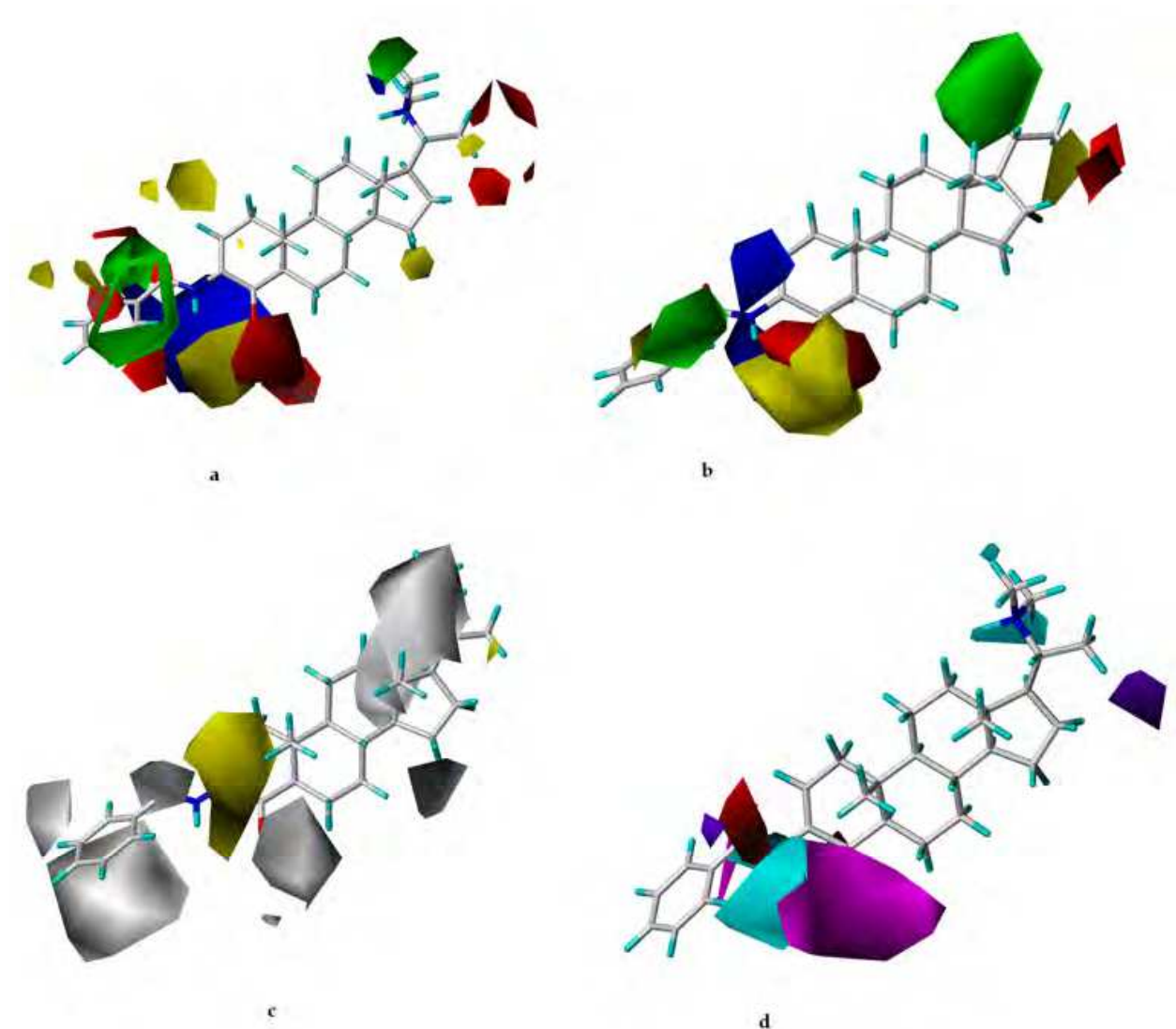


Fig. 7. **a)** The CoMFA (stdev*coeff) steric and electrostatic contour plots for AChE modeling. The favorable steric areas in green; disfavored steric areas in yellow. The positive potential favored area in blue; positive potential disfavored areas in red. The most active compound in the series (SAR33) is shown as the reference compound. **b)** The CoMSIA (stdev*coeff) steric and electrostatic contour plots. Color scheme same as in figure 7a. The most active compound in the series (SAR33) is shown as the reference compound. **c)** The CoMSIA (stdev*coeff) hydrophobic contour plots. The favorable hydrophobic areas indicated by yellow color, whereas the disfavored hydrophobic areas are shown by white color. The most active compound (SAR33) is shown as the reference compound. **d)** The contour plots of the CoMSIA (stdev*coeff) H-bond donor and acceptor fields. The favorable H-bond donor in cyan; unfavorable H-bond donor in purple. The favorable H-bond acceptor in magenta; unfavorable H-bond acceptor in red. The most active compound (SAR33) is shown as the reference compound

3.2.4 Graphical interpretation of the results (CoMSIA)

3.2.4.1 BuChE

The CoMSIA steric and electrostatic fields based on PLS analyses are represented as 3D contour plots in Figure 6b. In the electrostatic contour map, positive charge can be appeared closer to the regions of positive coefficients (blue) and negative charge can be moved closer to the regions of negative coefficients (red). A close inspection of the electrostatic contour plots (Figure 6b), reveals that for the tested molecules the electropositive groups are more preferred and appearance of the blue regions near R4 zone, indicate that more positive charge group substituted at this zone on the parent skeleton will enhance the biological activity.

In the steric contour map, it can be seen that, the areas (green contour) correspond to regions where steric occupancy with bulky groups are preferred and the areas encompassed by yellow contour should be sterically avoided. For the studied compounds on ring A, there exist two contour areas, a larger favorable area near the group substituted at the C3 on the ring A, and at the opposite site, a relatively smaller unfavorable area. Due to the steric complementarity between receptor and inhibitor, the positions which are encompassing the green region are sterically preferred to produce good steric interactions with the receptor and hence increasing the inhibitory activity. By observing the steric contour map with the compound SAR29 (one of the most active compound; Table 2), it can be readily seen that the green contour covered the whole carbonyl and double bond region at the senecieryl group while the terminal substituent on double bond in senecieryl group is covered by yellow contour. The green area is indicating that bulky substituent at double bond but adjacent to the carbonyl position will enhance the biological activity. Similarly, a smaller terminal substituent on the double bond will enhance the inhibitory activity. For example, the structure of the compound SAR12 has relatively small substituent, in the form of $-NHCH_3$, at C3, while SAR35 has a bulky substituent in the form of senecieryl group, shows less inhibitory activity than compound SAR12. The same is observed if we compare the compound SAR25 with SAR35.

The contour map of hydrophobic properties indicates (Figure 6c) one distinct hydrophobically favorable site, a larger region near the R2 zone, which means that groups with high hydrophobicity (indicated by yellow contour in Figure 6c) will favor biological activity. It can be reasonably presumed that ring A combined with a substituent on it, is composed of a large hydrophobic core, and will produce a strong hydrophobic interaction with the receptor. This observation is also consistent with the CoMFA steric contour map (Figure 6a) in which the sterically more crowded substituent is necessary to enhance the biological activity at the same R2 zone (see Figure 8 for R zones descriptions).

The graphical interpretations of the field contributions of the H-bond properties are shown in Figure 6d as both H-bond donor and H-bond acceptor fields. In principle, they should highlight the areas beyond the ligands where putative hydrogen partners in the enzyme can form H-bonds that influence binding affinity. The hydrogen bond donor and acceptor fields showed the favorable (cyan) area near the amido group and the H-bond acceptor field showed the favorable (magenta) area around the oxygen atom in amido group (Figure 6d). This may be due to the involvement of hydrogen bonding during interaction with target.

Superimposition of the CoMFA and CoMSIA coefficient contour maps on the ligand in the active site of BuChE (Figure 9a and 9b) additionally supports the result that most of the interactions are hydrophobic in nature and the residues nearby the hydrophobic favorable

area are mostly consisting of hydrophobic amino acids (i.e., Gly, Val, and Leu). As depicted in the figures 9a and 9b, the substituents at position R2 is placed in the hydrophobic pocket formed by Leu286, Gly116, Gly117, Val288, and Ala199. A green color contour map of CoMFA model (Figure 6a) and similarly of green contour of CoMSIA (Figure 6b) is appeared at this position suggesting for bulky substituents at this position. Another yellow color CoMSIA contour near the same R2 region suggesting the favorable hydrophobic interaction with the receptor hydrophobic pocket which is formed by the same amino acid residues. Most of the amino acid residues near the yellow contour regions are in hydrophobic in nature e.g., Gly, Val, and Leu. The same is true when comparing the CoMFA and CoMSIA contour maps within the active site residues of acetylcholinesterase (Figure 9c and 9d)

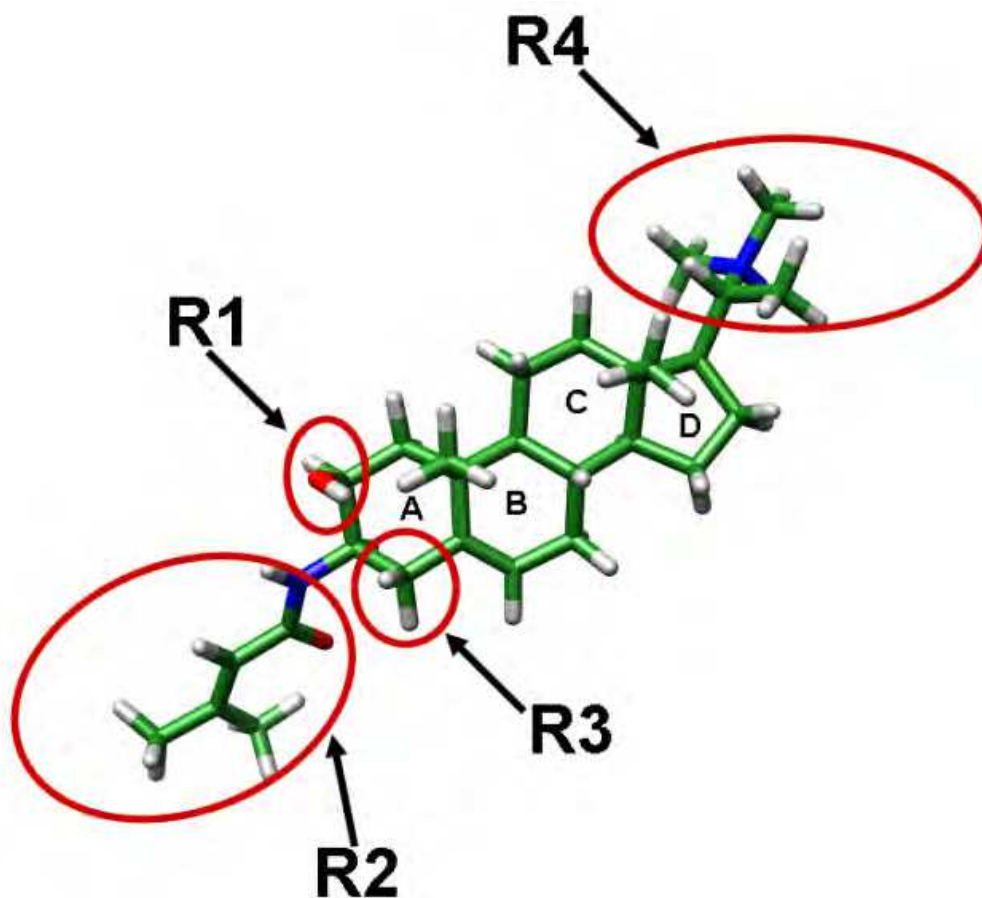


Fig. 8. An example of representative compound; showing important regions of the parent skeleton; circled here, as R1, R2, R3 and R4

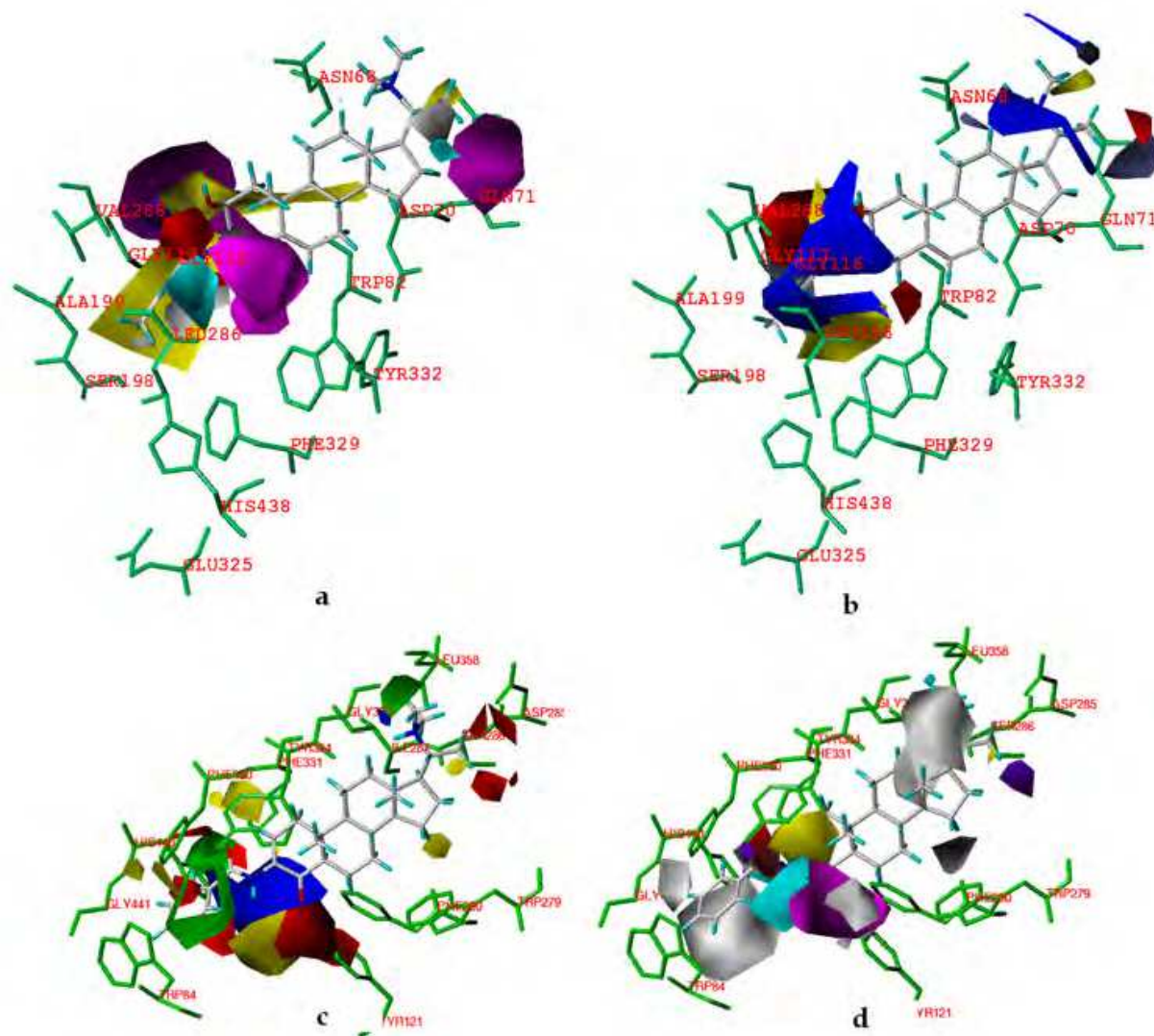


Fig. 9. a) CoMSIA contour plots superimposed within the active site of BuChE with compound SAR29 b) CoMFA contour plots superimposed within the active site of BuChE with compound SAR29 c) CoMFA contour plots superimposed within the active site of AChE with compound SAR33 d) CoMSIA contour plots superimposed within the active site of AChE with compound SAR33

3.2.4.2 AChE

The CoMSIA steric and electrostatic descriptors (Figure 7b) for the set of AChE inhibitors remain similar as the CoMFA and hence not described further. The CoMSIA hydrophobic descriptors are presented as contour maps in Figure 7c. The contour map of hydrophobic properties indicates a favourable region around the substituents as R2 (yellow contours in Figure 7c), pointing the hydrophobic groups is advantageous for the AChE inhibitory activity. The graphical interpretations of the H-bond properties are shown in Figure 7d. The contours present in the Figure 7d signify the importance of H-bond donor and acceptor characters in the region. In principle, almost all compounds have amide group present in the region and hence presence of these contours is correlated with potentially donor and acceptor amide group.

4. Conclusion

Present study correlates the cholinesterase inhibitory activities of isolated natural compounds with the steric, electrostatic and hydrophobicity parameters. Statistically significant 3D-QSAR models of the steroidal alkaloids inhibitors were designed by exploring multiple conformations of each ligand using the genetic algorithm. An alignment technique scheme was generated from the docking results and it yielded highly predictive 3D-QSAR models. The good correlation observed in all cases of 3D-QSAR supports the proposed method of alignment and selection of conformers.

Final models were validated by the prediction of inhibitory activities of the test set compounds. In terms of external predictions, CoMSIA and CoMFA both performed great. A comparison of the 3D-QSAR PLS coefficient contour maps with the structural and functional features of the binding sites also showed good correlation. It is evident from the contour plots of both analyses that the hydrophobic effect plays main contribution to the cholinesterase inhibitory activity and it's quite in agreement with the fact that the cholinesterases are having a wide active site gorge lining with hydrophobic amino acid residues. Also, bulky groups in the side chain at R2 position generally cause the increase in activity but at the same time the bulkier substituent at position R3 resulted in decreasing the activity. This R3 position is covered by a yellow steric contour and hence the bulkiness at this region is detrimental to the activity. The preference for bulky group at position R2 as described in CoMFA, seems to be correlated in CoMSIA with increased hydrophobicity expected at the same region. As an attempt to exploiting the cholinesterase inhibitors for 3D-QSAR approach combined with all detailed information obtained by 3D-QSAR models, we strongly believe that this study can help to design novel molecules with improved activity in near future.

The results, together with the good correlations between the actual and predicted inhibitory activities, demonstrate the power of combined docking/QSAR approach to explore the probable binding conformations of compounds at the active sites of the protein target. Additionally, present study also demonstrates that charges resulting from different calculation methods may influence the results of CoMFA as well as CoMSIA, although in our case this effect has not been significant. This is evident from the q^2 values calculated for different charge calculation methods (Table 4).

5. Acknowledgment

Financial support from Higher Education Commission, Pakistan to Uddin, R., under Split PhD program is highly acknowledged. The authors are thankful to Dr. Michael A Brunsteiner, Dr. Hongbin Yuan and Dr. Pavel A Petukhov from University of Illinois at Chicago for their help in developing the GA scripts in SPL and Perl languages. Authors are also thankful to S. T. Moin for assisting during the calculation runs. Authors are grateful to the Pakistan Science Foundation (PSF) for financial support to develop computational chemistry software facilities at the ICCBS.

Authors are also thankful to the OpenEye for providing us free academic license.

6. References

- Atta ur, R.; Choudhary, M. I.; Khan, M. R.; Anjum, S.; Farooq, A. & Iqbal, M. Z. (2000). New Steroidal Alkaloids from *Sarcococca saligna*. *Journal of Natural Products*, Vol.63, No.10, (October 2000), pp. 1364-8, ISSN 0163-3864

- Atta ur, R.; Feroz, F.; Naeem, I.; Zaheer ul, H.; Nawaz, S. A.; Khan, N.; Khan, M. R. & Choudhary, M. I. (2004). New Pregnane-type Steroidal Alkaloids from *Sarcococca saligna* and their Cholinesterase Inhibitory Activity. *Steroids*, Vol.69, No.11-12, (October-November 2004), pp. 735-41, ISSN 0039-128X
- Atta ur, R.; Feroz, F.; Zaheer ul, H.; Nawaz, S. A.; Khan, M. R. & Choudhary, M. I. (2003). New Steroidal Alkaloids from *Sarcococca saligna*. *Natural Product Research*, Vol.17, No.4, (August 2003), pp. 235-41, ISSN 1478-6419
- Atta ur, R.; Nasreen, A.; Akhtar, F.; Shekhani, M. S.; Clardy, J.; Parvez, M. & Choudhary, M. I. (1997). Antifungal Diterpenoid Alkaloids from *Delphinium denudatum*. *Journal of Natural Products*, Vol.60, No.5, (May 1997), pp. 472-474, ISSN 0163-3864
- Atta ur, R.; Zaheer ul, H.; Feroz, F.; Khalid, A.; Nawaz, S. A.; Khan, M. R. & Choudhary, M. I. (2004). New Cholinesterase-Inhibiting Steroidal Alkaloids from *Sarcococca saligna*. *Helvetica Chimica Acta*, Vol.87, No.2, (February 2004), pp. 439, ISSN 1522-2675
- Atta ur, R.; Zaheer ul, H.; Khalid, A.; Anjum, S.; Khan, M. R. & Choudhary, M. I. (2002). Pregnane-type Steroidal Alkaloids of *Sarcococca saligna*: A New Class of Cholinesterases Inhibitors. *Helvetica Chimica Acta*, Vol.85, No.2, (February 2002), pp. 678-688, ISSN 1522-2675
- Bazelyansky, M.; Robey, E. & Kirsch, J. F. (1986). Fractional diffusion-limited component of reactions catalyzed by acetylcholinesterase. *Biochemistry*, Vol.25, No.1, (January 1986), pp. 125-30, ISSN 0006-2960
- Behra, M.; Cousin, X.; Bertrand, C.; Vonesch, J. L.; Biellmann, D.; Chatonnet, A. & Strahle, U. (2002). Acetylcholinesterase is Required for Neuronal and Muscular Development in the Zebrafish Embryo. *Nature Neuroscience*, Vol.5, No.2, (February 2002), pp. 111-8, ISSN 1097-6256
- Bohm, M.; St rzebecher, J. & Klebe, G. (1999). Three-Dimensional Quantitative Structure-Activity Relationship Analyses using Comparative Molecular Field Analysis and Comparative Molecular Similarity Indices Analysis to Elucidate Selectivity Differences of Inhibitors Binding to Trypsin, Thrombin, and Factor Xa. *Journal of Medicinal Chemistry*, Vol.42, No.3, (February 1999), pp. 458-77, ISSN 0022-2623
- Bourne, Y.; Taylor, P. & Marchot, P. (1995). Acetylcholinesterase Inhibition by Fasciculin: Crystal Structure of the Complex. *Cell*, Vol.83, No.3, (November 1995), pp. 503-12, ISSN 0092-8674
- Buolamwini, J. K. & Assefa, H. (2002). CoMFA and CoMSIA 3D QSAR and Docking Studies on Conformationally-Restrained Cinnamoyl HIV-1 Integrase Inhibitors: Exploration of a Binding Mode at the Active Site. *Journal of Medicinal Chemistry*, Vol.45, No.4, (February 2002), pp. 841-852, ISSN 0022-2623
- Butters, N.; Delis, D. C. & Lucas, J. A. (1995). Clinical Assessment of Memory Disorders in Amnesia and Dementia. *Annual Review of Psychology*, Vol.46, (February 1995), pp. 493-523, ISSN 0066-4308
- Chatonnet, A. & Lockridge, O. (1989). Comparison of Butyrylcholinesterase and Acetylcholinesterase. *The Biochemical Journal*, Vol.260, No.3, (June 1989), pp. 625-34, ISSN 0264-6021
- Cho, S. J.; Garsia, M. L.; Bier, J. & Tropsha, A. (1996). Structure-Based Alignment and Comparative Molecular Field Analysis of Acetylcholinesterase Inhibitors. *Journal of Medicinal Chemistry*, Vol.39, No.26, (December 1996), pp. 5064-71, ISSN 0022-2623

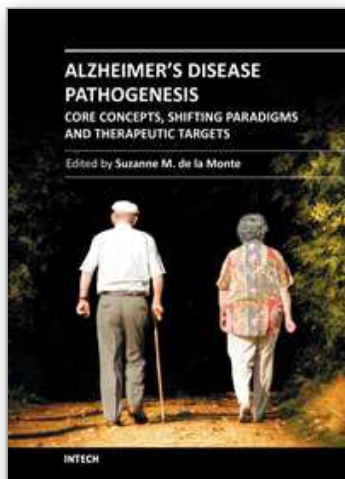
- Clark, M.; Cramer, R. D. & Van Opdenbosch, N. (1989). Validation of the General Purpose Tripos 5. 2 Force Field. *Journal of Computational Chemistry*, Vol.10, No.8, (December 1989), pp. 982-1012, ISSN 1096-987X
- Cokugras, A. N. (2003). Butyrylcholinesterase: Structure and Physiological Importance. *Turkish Journal of Biochemistry*, Vol.28, No.2, (October 2003), pp. 54-61, ISSN 0250-4685
- Cramer Iii, R. D.; Patterson, D. E. & Bunce, J. D. (1988). Comparative Molecular Field Analysis (CoMFA). 1. Effect of Shape on Binding of Steroids to Carrier Proteins. *Journal of the American Chemical Society*, Vol.110, No.18, (August 1988), pp. 5959-5967, ISSN 0002-7863
- Debnath, A. K. (1999). Three-Dimensional Quantitative Structure-Activity Relationship Study on Cyclic Urea Derivatives as HIV-1 Protease Inhibitors: Application of Comparative Molecular Field Analysis. *Journal of Medicinal Chemistry*, Vol.42, No.2, (January 1999), pp. 249-59, ISSN 0022-2623
- Dominguez, C.; Boelens, R. & Bonvin, A. M. (2003). HADDOCK: A Protein-Protein Docking Approach Based on Biochemical or Biophysical Information. *Journal of American Chemical Society*, Vol.125, No.7, (Feb 19), pp. 1731-7, ISSN 0002-7863
- Donini, O. A. & Kollman, P. A. (2000). Calculation and Prediction of Binding Free Energies for the Matrix Metalloproteinases. *Journal of Medicinal Chemistry*, Vol.43, No.22, (November 2000), pp. 4180-8, ISSN 0022-2623
- Doorn, J. A.; Talley, T. T.; Thompson, C. M. & Richardson, R. J. (2001). Probing the Active Sites of Butyrylcholinesterase and Cholesterol Esterase with Isomalathion: Conserved Stereoselective Inactivation of Serine Hydrolases Structurally Related to Acetylcholinesterase. *Chemical Research in Toxicology*, Vol.14, No.7, (July 2001), pp. 807-13, ISSN 0893-228X
- Fogel, L. J.; Owens, A. J. & Walsh, M. J. (1966). *Artificial Intelligence Through Simulated Evolution*, Wiley, New York
- Forrest, S. (1993). Genetic Algorithms: Principles of Natural Selection Applied to Computation. *Science*, Vol.261, No.5123, (August 1993), pp. 872, ISSN 0036-8075
- FRED (2007). FRED, version 2.2.3, OpenEye Scientific Software, Inc., Santa Fe, NM, USA, www.eyesopen.com, 2007. pp.
- Geladi, P. & Kowalski, B. R. (1986). Partial Least Squares: A Tutorial. *Analytica Chimica Acta*, Vol.185, (July 1986), pp. 1-17, ISSN 0003-2670
- Giacobini, E. (2003). Cholinesterases: New Roles in Brain Function and in Alzheimer's Disease. *Neurochemical Research*, Vol.28, No.3-4, (April 2003), pp. 515-22, ISSN 0364-3190
- Giacobini, E. (1964). Metabolic Relations Between Glia and Neurons Studied in Single Cells, In: *Morphological and Biochemical Correlates of Neural Activity*, pp. 15-38, Harper & Row, ISBN 978-006-1406-40-9, New York, USA
- Goldberg, D. E. (1989). *Genetic Algorithm in Search, Optimization and Machine Learning*, Addison-Wesley Professional, ISBN 978-020-1157-673, Reading, MA
- Graybiel, A. M. & Ragsdale, C. W., Jr. (1982). Pseudocholinesterase Staining in the Primary Visual Pathway of the Macaque Monkey. *Nature*, Vol.299, No.5882, (September 1982), pp. 439-42, ISSN 0028-0836
- Greig, N. H.; Utsuki, T.; Yu, Q.; Zhu, X.; Holloway, H. W.; Perry, T.; Lee, B.; Ingram, D. K. & Lahiri, D. K. (2001). A New Therapeutic Target in Alzheimer's Disease Treatment:

- Attention to Butyrylcholinesterase. *Current Medical Research and Opinion*, Vol.17, No.3, pp. 159-65, ISSN 0300-7995
- Guillozet, A. L.; Smiley, J. F.; Mash, D. C. & Mesulam, M. M. (1997). Butyrylcholinesterase in the Life Cycle of Amyloid Plaques. *Annals of Neurology*, Vol.42, No.6, (December 1997), pp. 909-18, ISSN 0364-5134
- Harel, M.; Sussman, J. L.; Krejci, E.; Bon, S.; Chanal, P.; Massoulie, J. & Silman, I. (1992). Conversion of Acetylcholinesterase to Butyrylcholinesterase: Modeling and Mutagenesis. *Proceedings of the National Academy of Sciences of the United States of America*, Vol.89, No.22, (November 1992), pp. 10827-31, ISSN 0027-8424
- Holland, J. H. (1975). *Adaptation in Natural and Artificial Systems*, University of Michigan press, ISBN 978-026-2581-11-0, Ann Arbor, MI
- Hu, X. & Stebbins, C. E. (2005). Molecular Docking and 3D-QSAR Studies of Yersinia Protein Tyrosine Phosphatase YopH Inhibitors. *Bioorganic and Medicinal Chemistry*, Vol.13, No.4, (February 2005), pp. 1101-9, ISSN 0968-0896
- Jain, A. N. (2003). Surfex: Fully Automatic Flexible Molecular Docking using a Molecular Similarity-Based Search Engine. *Journal of Medicinal Chemistry*, Vol.46, No.4, (February 2003), pp. 499-511, ISSN 0022-2623
- Johnson, M. A.; Hoog, C. & Pinto, B. M. (2003). A Novel Modeling Protocol for Protein Receptors Guided by Bound-Ligand Conformation. *Biochemistry*, Vol.42, No.7, (February 2003), pp. 1842-53, ISSN 0006-2960
- Kalauni, S. K.; Choudhary, M. I.; Shaheen, F.; Manandhar, M. D.; Atta ur, R.; Gewali, M. B. & Khalid, A. (2001). Steroidal Alkaloids from the Leaves of *Sarcococca coriacea* of Nepalese Origin. *Journal of Natural Products*, Vol.64, No.6, (June 2001), pp. 842-4, ISSN 0163-3864
- Khalid, A.; Zaheer ul, H.; Anjum, S.; Khan, M. R.; Atta ur, R. & Choudhary, M. I. (2004). Kinetics and Structure-Activity Relationship Studies on Pregnane-Type Steroidal Alkaloids that Inhibit Cholinesterases. *Bioorganic and Medicinal Chemistry*, Vol.12, No.9, (May 1), pp. 1995-2003, ISSN 0968-0896
- Khalid, A.; Zaheer ul, H.; Ghayur, M. N.; Feroz, F.; Atta ur, R.; Gilani, A. H. & Choudhary, M. I. (2004). Cholinesterase Inhibitory and Spasmolytic Potential of Steroidal Alkaloids. *Journal of Steroid Biochemistry and Molecular Biology*, Vol.92, No.5, (December 2004), pp. 477-84, ISSN 0960-0760
- Klebe, G. (1998). Comparative Molecular Similarity Indices Analysis: CoMSIA, In: *3D QSAR in Drug Design: Recent Advances*, pp. 87-104, Kluwer Academic Publishers, ISBN 978-904-8149-35-3, London
- Klebe, G.; Abraham, U. & Mietzner, T. (1994). Molecular Similarity Indices in a Comparative Analysis (CoMSIA) of Drug Molecules to Correlate and Predict their Biological Activity. *Journal of Medicinal Chemistry*, Vol.37, No.24, (November 1994), pp. 4130-46, ISSN 0022-2623
- Lemmen, C.; Lengauer, T. & Klebe, G. (1998). FLEXS: A Method for Fast Flexible Ligand Superposition. *Journal of Medicinal Chemistry*, Vol.41, No.23, (October 1998), pp. 4502-4520, ISSN 0022-2623
- Lockridge, O. & Masson, P. (2000). Pesticides and Susceptible Populations: People with Butyrylcholinesterase Genetic Variants may be at Risk. *Neurotoxicology*, Vol.21, No.1-2, (February-April 2000), pp. 113-26, ISSN 0161-813X

- Mack, A. & Robitzki, A. (2000). The Key Role of Butyrylcholinesterase during Neurogenesis and Neural Disorders: An Antisense-5'Butyrylcholinesterase-DNA Study. *Progress in Neurobiology*, Vol.60, No.6, (April 2000), pp. 607-28, ISSN 0301-0082
- Massoulie, J.; Pezzementi, L.; Bon, S.; Krejci, E. & Vallette, F. M. (1993). Molecular and Cellular Biology of Cholinesterases. *Progress in Neurobiology*, Vol.41, No.1, (July 1993), pp. 31-91, ISSN 0301-0082
- Massoulie, J.; Sussman, J.; Bon, S. & Silman, I. (1993). Cholinergic Function and Dysfunction: Structure and Functions of Acetylcholinesterase and Butyrylcholinesterase, In: *Progress in Brain Research*, pp. 139-46, ISBN 978-044-4897-17-6,
- McGann, M. R.; Almond, H. R.; Nicholls, A.; Grant, J. A. & Brown, F. K. (2003). Gaussian Docking Functions. *Biopolymers*, Vol.68, No.1, pp. 76-90, ISSN 1097-0282
- Medina-Franco, J. L.; Rodríguez-Morales, S.; Juárez-Gordiano, C.; Hernández-Campos, A. & Castillo, R. (2004). Docking-Bbased CoMFA and CoMSIA Studies of Non-Nucleoside Reverse Transcriptase Inhibitors of the Pyridinone Derivative Type. *Journal of Computer-Aided Molecular Design*, Vol.18, No.5, (July 2004), pp. 345-360, ISSN 0920-654X
- Meshorer, E.; Erb, C.; Gazit, R.; Pavlovsky, L.; Kaufer, D.; Friedman, A.; Glick, D.; Ben-Arie, N. & Soreq, H. (2002). Alternative Splicing and Neuritic mRNA Translocation Under Long-Term Neuronal Hypersensitivity. *Science*, Vol.295, No.5554, (January 2002), pp. 508-12, ISSN 0036-8075
- Nachon, F.; Asojo, O. A.; Borgstahl, G. E.; Masson, P. & Lockridge, O. (2005). Role of Water in Aging of Human Butyrylcholinesterase Inhibited by Echothiophate: The Crystal Structure Suggests Two Alternative Mechanisms of Aging. *Biochemistry*, Vol.44, No.4, (February 2005), pp. 1154-62, ISSN 0006-2960
- Nachon, F.; Nicolet, Y. & Masson, P. (2005). Butyrylcholinesterase: 3D structure, Catalytic Mechanisms. *Annales Pharmaceutiques Francaises*, Vol.63, No.3, (June 2005), pp. 194-206, ISSN 0003-4509
- Nicolet, Y.; Lockridge, O.; Masson, P.; Fontecilla-Camps, J. C. & Nachon, F. (2003). Crystal Structure of Human Butyrylcholinesterase and of Its Complexes with Substrate and Products. *Journal of Biological Chemistry*, Vol.278, No.42, (October 2003), pp. 41141-7, ISSN 0021-9258
- OE ROCS, v. (2008). OpenEye Scientific Software, Inc., Santa Fe, NM, USA, www.eyesopen.com, 2008. pp.
- Pan, X.; Tan, N.; Zeng, G.; Han, H. & Huang, H. (2006). 3D-QSAR and Docking Studies of Aldehyde Inhibitors of Human Cathepsin K. *Bioorganic and Medicinal Chemistry*, Vol.14, No.8, (April 2006), pp. 2771-2778, ISSN 0968-0896
- Perry, E. K.; Tomlinson, B. E.; Blessed, G.; Bergmann, K.; Gibson, P. H. & Perry, R. H. (1978). Correlation of Cholinergic Abnormalities with Senile Plaques and Mental Test Scores in Senile Dementia. *British Medical Journal*, Vol.2, No.6150, (November 1978), pp. 1457-1459, ISSN 1759-2151
- Prathipati, P.; Pandey, G. & Saxena, A. K. (2005). CoMFA and Docking Studies on Glycogen Phosphorylase a Inhibitors as Antidiabetic Agents. *Journal of Chemical Information and Modeling*, Vol.45, No.1, (Jan-Feb 2005), pp. 136-45, ISSN 1549-9596
- Radic, Z.; Pickering, N. A.; Vellom, D. C.; Camp, S. & Taylor, P. (1993). Three Distinct Domains in the Cholinesterase Molecule Confer Selectivity for Acetyl- and

- Butyrylcholinesterase Inhibitors. *Biochemistry*, Vol.32, No.45, (November 1993), pp. 12074-84, ISSN 0006-2960
- Rarey, M.; Kramer, B.; Lengauer, T. & Klebe, G. (1996). A Fast Flexible Docking Method Using an Incremental Construction Algorithm. *Journal of Molecular Biology*, Vol.261, No.3, (August 1996), pp. 470-489, ISSN 0022-2836
- Sabnis, Y. A.; Desai, P. V.; Rosenthal, P. J. & Avery, M. A. (2003). Probing the Structure of Falcipain-3, A Cysteine Protease from *Plasmodium falciparum*: Comparative Protein Modeling and Docking Studies. *Protein Science*, Vol.12, No.3, (March 2003), pp. 501-9, ISSN 0961-8368
- Saxena, A.; Redman, A. M.; Jiang, X.; Lockridge, O. & Doctor, B. P. (1999). Differences in Active-Site Gorge Dimensions of Cholinesterases Revealed by Binding of Inhibitors to Human Butyrylcholinesterase. *Chemico-Biological Interactions*, Vol.119-120, (May 1999), pp. 61-9, ISSN 0009-2797
- Saxena, A.; Redman, A. M.; Jiang, X.; Lockridge, O. & Doctor, B. P. (1997). Differences in Active Site Gorge Dimensions of Cholinesterases Revealed by Binding of Inhibitors to Human Butyrylcholinesterase. *Biochemistry*, Vol.36, No.48, (December 1997), pp. 14642-51, ISSN 0006-2960
- Soreq, H. & Zaku, H. (1993). *Human Cholinesterases and Anticholinesterases*, Academic Press, ISBN 978-012-6552-90-4, San Diego, USA
- Sussman, J. L.; Harel, M.; Frolow, F.; Oefner, C.; Goldman, A.; Toker, L. & Silman, I. (1991). Atomic Structure of Acetylcholinesterase from *Torpedo californica*: A Prototypic Acetylcholine-Binding Protein. *Science*, Vol.253, No.5022, (August 1991), pp. 872-9, ISSN 0036-8075
- Sybyl, V. (2007). 7.3, Tripos Inc, St. Louis, MO, pp.
- Tame, J. R. (1999). Scoring Functions: A View from the Bench. *Journal of Computer-Aided Molecular Design*, Vol.13, No.2, (March 1999), pp. 99-108, ISSN 0920-654X
- Terry, A. V., Jr. & Buccafusco, J. J. (2003). The Cholinergic Hypothesis of Age and Alzheimer's Disease-Related Cognitive Deficits: Recent Challenges and their Implications for Novel Drug Development. *The Journal of Pharmacology and Experimental Therapeutics*, Vol.306, No.3, (September 2003), pp. 821-27, ISSN 0022-3565
- Todorov, N. P.; Mancera, R. L. & Monthoux, P. H. (2003). A New Quantum Stochastic Tunnelling Optimisation Method for Protein-Ligand Docking *Chemical Physics Letters*, Vol.369, No.3-4, (February 2003), pp. 257-263, ISSN 0009-2614
- Tormos, J. R.; Wiley, K. L.; Seravalli, J.; Nachon, F.; Masson, P.; Nicolet, Y. & Quinn, D. M. (2005). The Reactant State for Substrate-Activated Turnover of Acetylthiocholine by Butyrylcholinesterase is a Tetrahedral Intermediate. *Journal of the American Chemical Society*, Vol.127, No.42, (October 2005), pp. 14538-9, ISSN 0002-7863
- Vicker, N.; Ho, Y.; Robinson, J.; Woo, L. L.; Purohit, A.; Reed, M. J. & Potter, B. V. (2003). Docking Studies of Sulphamate Inhibitors of Estrone Sulphatase in Human Carbonic Anhydrase II. *Bioorganic Medicinal Chemistry Letters*, Vol.13, No.5, (March 2003), pp. 863-5, ISSN 0960-894X
- Viswanadhan, V. N.; Ghose, A. K.; Revankar, G. R. & Robins, R. K. (1989). Atomic Physicochemical Parameters for Three Dimensional Structure Directed Quantitative Structure-Activity Relationships. 4. Additional Parameters for Hydrophobic and Dispersive Interactions and their Application for an Automated Superposition of

- Certain Naturally Occurring Nucleoside Antibiotics. *Journal of Chemical Information and Computer Sciences*, Vol.29, No.3, (August 1989), pp. 163 - 172, ISSN 1549-9596
- Wang, L.; Merz, A. J.; Collins, K. M. & Wickner, W. (2003). Hierarchy of Protein Assembly at the Vertex Ring Domain for Yeast Vacuole Docking and Fusion. *Journal of Cell Biology*, Vol.160, No.3, (February 2003), pp. 365-74, ISSN 0021-9525
- Wei, H. Y.; Tsai, K. C. & Lin, T. H. (2005). Modeling Ligand- Receptor Interaction for Some MHC Class II HLA-DR4 Peptide Mimetic Inhibitors Using Several Molecular Docking and 3D QSAR Techniques. *Journal of Chemical Information and Modeling*, Vol.45, No.5, (September-October 2005), pp. 1343-1351, ISSN 1549-9596
- Wu, X.; Milne, J. L.; Borgnia, M. J.; Rostapshov, A. V.; Subramaniam, S. & Brooks, B. R. (2003). A Core-Weighted Fitting Method for Docking Atomic Structures into Low-Resolution Maps: Application to Cryo-Electron Microscopy. *Journal of Structural Biology*, Vol.141, No.1, (January 2003), pp. 63-76, ISSN 1047-8477
- Xie, W.; Stribley, J. A.; Chatonnet, A.; Wilder, P. J.; Rizzino, A.; McComb, R. D.; Taylor, P.; Hinrichs, S. H. & Lockridge, O. (2000). Postnatal Developmental Delay and Supersensitivity to Organophosphate in Gene-Targeted Mice Lacking Acetylcholinesterase. *Journal of Pharmacology and Experimental Therapeutics*, Vol.293, No.3, (June 2000), pp. 896-902, ISSN 0022-3565
- Yuan, H.; Kozikowski, A. P. & Petukhov, P. A. (2004). CoMFA Study of Piperidine Analogues of Cocaine at the Dopamine Transporter: Exploring the Binding Mode of the 3 Alpha-Substituent of the Piperidine Ring Using Pharmacophore-Based Flexible Alignment. *Journal of Medicinal Chemistry*, Vol.47, No.25, (December 2004), pp. 6137-43, ISSN 0022-2623
- Yuan, H. & Petukhov, P. A. (2006). Improved 3D-QSAR CoMFA of the Dopamine Transporter Blockers with Multiple Conformations Using the Genetic Algorithm. *Bioorganic and Medicinal Chemistry Letters*, Vol.16, No.24, (December 2006), pp. 6267-72, ISSN 0960-894X
- Zaheer-Ul-Haq; Wellenzohn, B.; Liedl, K. R. & Rode, B. M. (2003). Molecular Docking Studies of Natural Cholinesterase-Inhibiting Steroidal Alkaloids from *Sarcococca saligna*. *Journal of Medicinal Chemistry*, Vol.46, No.23, (November 2003), pp. 5087-90, ISSN 0022-2623
- Zaheer ul, H.; Uddin, R.; Yuan, H.; Petukhov, P. A.; Choudhary, M. I. & Madura, J. D. (2008). Receptor-based modeling and 3D-QSAR for a quantitative production of the butyrylcholinesterase inhibitors based on genetic algorithm. *Journal of Chemical Information and Modeling*, Vol.48, No.5, pp. 1092-1103, ISSN 1549-9596
- Zaheer ul, H.; Wellenzohn, B.; Tonmunphean, S.; Khalid, A.; Choudhary, M. I. & Rode, B. M. (2003). 3D-QSAR Studies on Natural Acetylcholinesterase inhibitors of *Sarcococca saligna* by comparative molecular field analysis (CoMFA). *Bioorg Med Chem Lett*, Vol.13, No.24, (Dec 15), pp. 4375-80, ISSN 0960-894X
- Zhou, Z.; Fisher, D.; Spidel, J.; Greenfield, J.; Patson, B.; Fazal, A.; Wigal, C.; Moe, O. A. & Madura, J. D. (2003). Kinetic and Docking Studies of the Interaction of Quinones with the Quinone Reductase Active Site. *Biochemistry*, Vol.42, No.7, (February 2003), pp. 1985-94, ISSN 0006-2960



Alzheimer's Disease Pathogenesis-Core Concepts, Shifting Paradigms and Therapeutic Targets

Edited by Dr. Suzanne De La Monte

ISBN 978-953-307-690-4

Hard cover, 686 pages

Publisher InTech

Published online 12, September, 2011

Published in print edition September, 2011

Alzheimer's Disease Pathogenesis: Core Concepts, Shifting Paradigms, and Therapeutic Targets, delivers the concepts embodied within its title. This exciting book presents the full array of theories about the causes of Alzheimer's, including fresh concepts that have gained ground among both professionals and the lay public. Acknowledged experts provide highly informative yet critical reviews of the factors that most likely contribute to Alzheimer's, including genetics, metabolic deficiencies, oxidative stress, and possibly environmental exposures. Evidence that Alzheimer's resembles a brain form of diabetes is discussed from different perspectives, ranging from disease mechanisms to therapeutics. This book is further energized by discussions of how neurotransmitter deficits, neuro-inflammation, and oxidative stress impair neuronal plasticity and contribute to Alzheimer's neurodegeneration. The diversity of topics presented in just the right depth will interest clinicians and researchers alike. This book inspires confidence that effective treatments could be developed based upon the expanding list of potential therapeutic targets.

How to reference

In order to correctly reference this scholarly work, feel free to copy and paste the following:

Zaheer ul Haq and Reaz Uddin (2011). Structure Based 3D-QSAR Studies on Cholinesterase Inhibitors, Alzheimer's Disease Pathogenesis-Core Concepts, Shifting Paradigms and Therapeutic Targets, Dr. Suzanne De La Monte (Ed.), ISBN: 978-953-307-690-4, InTech, Available from:

<http://www.intechopen.com/books/alzheimer-s-disease-pathogenesis-core-concepts-shifting-paradigms-and-therapeutic-targets/structure-based-3d-qsar-studies-on-cholinesterase-inhibitors>

INTECH
open science | open minds

InTech Europe

University Campus STeP Ri
Slavka Krautzeka 83/A
51000 Rijeka, Croatia
Phone: +385 (51) 770 447
Fax: +385 (51) 686 166
www.intechopen.com

InTech China

Unit 405, Office Block, Hotel Equatorial Shanghai
No.65, Yan An Road (West), Shanghai, 200040, China
中国上海市延安西路65号上海国际贵都大饭店办公楼405单元
Phone: +86-21-62489820
Fax: +86-21-62489821

© 2011 The Author(s). Licensee IntechOpen. This chapter is distributed under the terms of the [Creative Commons Attribution-NonCommercial-ShareAlike-3.0 License](#), which permits use, distribution and reproduction for non-commercial purposes, provided the original is properly cited and derivative works building on this content are distributed under the same license.

IntechOpen

IntechOpen